YAP1-2α/TAZ heterodimerization drives phase separation, activating TEAD-positive super-enhancers that enhance cancer stemness and multidrug resistance

Takuya Ooki[1], Takeru Hayashi[1], Yui Yamamoto[1] & Masanori Hatakeyama[1,2,*]

[1]Laboratory of Microbial Carcinogenesis, Institute of Microbial Chemistry, Microbial Chemistry Research Foundation, Tokyo, Japan

[2]Center of Infection-associated Cancer, Institute for Genetic Medicine, Hokkaido University, Sapporo, Japan

***e-mail: mhata@m.u-tokyo.ac.jp**

ABSTRACT

The acquisition of drug resistance poses a significant challenge for successful cancer treatment. Understanding the mechanisms by which cancer evades drug action is crucial for developing effective therapies. PARP inhibitors (PARPi) induce synthetic lethality in *BRCA*-deficient cancer cells; however, these cells eventually develop PARPi resistance. Here, we demonstrate that prolonged exposure of *BRCA*-deficient cancer cells to PARPi or Cisplatin leads to alterations in *YAP1* pre-mRNA splicing patterns, resulting in selective upregulation of a minor YAP1 isoform, YAP1-2α. Elevated YAP1-2α specifically heterodimerizes with TAZ, triggering liquid-liquid phase separation (LLPS). This process generates nuclear condensates that activate super-enhancers containing the YAP1-2α/TAZ heterodimer, TEAD, and BRD4. These super-enhancers (here referred to as YAP1-2α/TAZ/TEAD super-enhancers) are also activated in CD44(variant)^{high} cancer stem-like populations in parental cells. In both PARPi-resistant and CD44(variant)^{high} cancer cell populations, treatments that disrupt YAP1-2α/TAZ/TEAD super-enhancers abolish cancer stem-like properties. Thus, the activation of YAP1-2α/TAZ/TEAD super-enhancers reinforces cancer cell stemness, which confers resistance to adverse conditions, such as those caused by anticancer drug treatment, including PARPi and Cisplatin. Our investigation reveals that YAP1-2α/TAZ/TEAD super-enhancers transcriptionally facilitate the malignant grade of cancer cells.

Disrupting these super-enhancers represents a promising strategy to hinder neoplastic progression and prevent multidrug resistance in cancer cells.

Introduction

Cancer cells employ various mechanisms to develop resistance to anticancer drugs, posing significant challenges in cancer treatment. These mechanisms include specific mutations altering drug binding sites[1], upregulation of ABC transporters enhancing drug efflux[2], and epigenetic modifications inducing changes in gene expression[3]. Recent studies have also highlighted the role of cancer stem-like cells (CSCs) in drug resistance, demonstrating their ability to withstand adverse conditions and various anticancer treatments[4]. CSCs exhibit increased robustness to unfavored conditions/stresses, which enhance their survival against a wide range of anticancer therapies. Importantly, differentiated cancer cells can revert into CSCs, a process often associated with epithelial-to-mesenchymal transition (EMT)[5]. EMT enhances cancer stem-like properties, contributing to increased invasion, metastasis, and resistance to cancer therapy[6].

The regulation of cancer stemness involves complex transcriptional networks, potentially mediated by super-enhancers[7]. Super-enhancers are characterized by high concentrations of transcription factors, co-activators, mediators, and epigenetic modifiers that robustly facilitate transcriptional output and integrate multiple signaling pathways that determine cell identity and status[8,9]. Master transcription factors co-occupy the super-enhancer and constitute a core regulatory circuitry to regulate cellular transcriptional programs[10]. Liquid-liquid phase separation (LLPS)-mediated condensation of transcription factors and co-

activators plays a crucial role in the formation and activation of super-enhancers[11]. Cancer cells utilize super-enhancers to adapt themselves to external environments by rewiring physiological transcriptional networks, potentiating malignant characteristics through aberrantly activating mitogenic signaling, anti-apoptotic machinery, migration/metastasis processes, and DNA repair systems, while creating tumor-favorable microenvironments, including immunosuppressive conditions[12-16]. Consequently, activation of super-enhancers endows resistance of cancer cells to various anticancer environments[17]. Among the multiple super-enhancers present in cells, those activated by the Hippo signal-regulated transcriptional coactivators, YAP1 and TAZ, are particularly significant in conferring cancer stem-like properties[18]. YAP1 and TAZ lack a DNA-binding domain; instead, they activate downstream transcription by interacting with sequence-specific transcription factors, most notably the TEAD family (TEAD1-4)[19,20]. The YAP-TEAD and TAZ-TEAD complexes integrate signals related to mechanical, metabolic, and cell density to coordinate cell proliferation and differentiation during development and neoplastic progression by activating classical and super-enhancers[21]. In cancer cells, YAP1 and TAZ contribute to resistance to anticancer drugs[22]. Critically, the transcriptional programs mediated by YAP1-TEAD and TAZ-TEAD intersect with the KRAS-ERK MAPK pathway, sharing target genes that confer resistance to RAF and MEK inhibitors in various cancer cells[23,24]. Additionally, elevated levels of the YAP1-TEAD and TAZ-TEAD complexes promote cancer stem-like properties through TEAD-dependent

transactivation of EMT-inducing transcriptional regulators such as ZEB1 and Slug[25]. While YAP1 and TAZ collaborate to control gene expression, their binding sites are not always identical or overlapping[26,27]. This observation suggests that the YAP1-TEAD and TAZ-TEAD transcriptional complexes may act on distinct subsets of enhancers and super-enhancers, with YAP1-bound super-enhancers comprising approximately 17% of all super-enhancers in the cell[28]. Intriguingly, the propensity of YAP1 and TAZ to undergo LLPS varies significantly. TAZ can induce LLPS through TAZ homodimerization via its leucine zipper motif in the coiled-coil domain[29]. In contrast, YAP1 does not readily induce LLPS due to its inability to undergo YAP1 homodimerization in the coiled-coil domain[29,30]. In this regard, we recently found that, among eight human YAP1 isoforms generated by differential splicing of *YAP1* pre-mRNA[31], only YAP1-1α and YAP1-2α contain a functional leucine zipper in the coiled-coil domain. These two YAP1 isoforms, but no other YAP1 isoforms, can heterodimerize with TAZ via leucine zippers[32].

The treatment of cancers with defective *BRCA1* or *BRCA2* (collectively referred to as *BRCA*-deficient cancers) induces synthetic lethality with poly ADP-ribose polymerase inhibitors (PARPi) or Cisplatin through excessive DNA double-strand break (DSB) induction[33]. However, *BRCA*-deficient cancer cells ultimately develop resistance to PARP1 or Cisplatin. In this study, we demonstrate that YAP1-2α is upregulated explicitly in *BRCA*-deficient cancer cells under genotoxic stress, such as prolonged treatment with PARPi or Cisplatin, due to a splice switching of

YAP1 pre-mRNAs from a *YAP1-2γ* mRNA dominance to a *YAP1-2α* mRNA dominance. The resulting YAP1-2α/TEAD complex associates with the TAZ/TEAD complex through leucine zipper-mediated YAP1-2α/TAZ heterodimerization, triggering the induction of LLPS, which then activates the YAP1-2α/TAZ/TEAD-specific super-enhancers. These super-enhancers reorganize the transcriptional network, enhancing cancer stem-like properties and conferring resistance to anticancer drugs beyond PARPi and Cisplatin. This study describes the unexpected connection between the splice switching of *YAP1* pre-mRNA, LLPS induction, and the activation of super-enhancers that confers cancer stem-like malignant properties. Inhibition of *YAP1-2α* mRNA splicing variant production or disruption of YAP1-2α/TAZ/TEAD super-enhancers may impede neoplastic progression and mitigate resistance to anticancer drugs.

Results

Establishment of PARPi-resistant cells from *BRCA*-deficient cancer cells

To elucidate the mechanism behind *BRCA*-deficient cancers' resistance to PARPi-induced synthetic lethality, we generated PARPi-resistant cells from two human *BRCA1*-mutated cancer cells: MDA-MB-436 triple-negative breast cancer and UWB1.289 serous ovarian cancer (Supplementary Fig. 1a). To assess drug resistance specificity, we exposed parental and PARPi-resistant cells to DNA-damaging agents (Olaparib, Cisplatin) and non-DNA-damaging agents (Paclitaxel, Staurosporine). Results showed that PARPi-resistant cells resisted Cisplatin but not Paclitaxel and Staurosporine, indicating acquired resistance to conventional DNA-damaging agents (Supplementary Fig. 1b, c, d).

We conducted RNA-sequencing (RNA-seq) analysis on PARPi-resistant cells derived from MDA-MB-436 and UWB1.289 and compared their gene expression profiles to those of parental cells (Fig. 1a). Gene ontology and hallmark gene set analyses were performed on 1,132 commonly upregulated genes in the resistant cells. PARPi resistance was linked to increased gene expression in innate immune/inflammatory responses such as SASP and enhanced cytokine/chemokine signaling, likely induced by cGAS-STING signaling from PARPi trapping-induced DNA damage[34]. RNA-seq data also showed elevated expression of genes related to EMT, suggesting dedifferentiation of the resistant cancer cells. This was supported by higher mRNA levels of YAP1 and TAZ signaling,

KRAS signaling, WNT signaling, anti-ROS signaling, and anti-apoptotic signaling. Additionally, genes associated with cell stemness were more highly expressed in PARPi-resistant cells than in parental cells (Supplementary Fig. 1e). The elevated expression of genes involved in recognizing and repairing DNA double-strand breaks, including error-prone microhomology-mediated end-joining (MMEJ) and single-strand annealing (SSA) (Fig. 1a), may explain the increased resistance of PARPi-resistant *BRCA*-deficient cancer cells to conventional DNA-damaging agents.

RNA-seq analysis also indicates that PARPi resistance in *BRCA*-deficient cancer cells stems from extensive transcriptional network restructuring that affects the expression of genes involved in various biological processes rather than a change in a small set of genes. To explore this, we examined YAP1 and TAZ transcriptional co-activators, as genes regulated by the TEAD transcription factors (TEAD1-4), the primary targets of YAP1 and TAZ, were significantly elevated in PARPi-resistant cells (Fig. 1b). *YAP1* pre-mRNA undergoes complex differential splicing, resulting in the production of eight YAP1 isoforms in human cells. (Supplementary Fig. 1f)[35]. The presence or absence of exon 4, encoding the second WW domain (WW2), classifies YAP1 into YAP1-1 (one WW domain) and YAP1-2 (two WW domains). The WW domain binds proline-containing sequences like PPxY[36]. There are four additional pre-mRNA splicing variants for both *YAP1-1* and *YAP1-2* species. *YAP1-1γ* and *YAP1-2γ* mRNAs contain a shorter exon 5 (exon 5.1, lacking the β-segment) and

exon 6. *YAP1-1δ* and *YAP1-2δ* mRNAs feature a more extended exon 5 (exon 5.2, including the β-segment) and exon 6 (encoding the γ-segment). *YAP1-1β* and *YAP1-2β* mRNAs have exon 5.2 but lack exon 6, while *YAP1-1α* and *YAP1-2α* mRNAs possess exon 5.1 but lack exon 6 (Supplementary Fig. 1f). Among these, only *YAP1-1α mRNA*-derived YAP1-1α and *YAP1-2α* mRNA-derived YAP1-2α isoforms have a functional Leucine zipper in the coiled-coil domain. To examine *YAP1* mRNA splicing patterns in *BRCA*-deficient cancer cells before and after acquiring PARPi resistance, we used RT-PCR to assess exon 6 inclusion or exclusion. We found that *YAP1* splicing variants including exon 6 were predominant in parental cells, whereas variants lacking exon 6 were prevalent in PARPi-resistant cells (Fig. 1c). Further splicing variant analysis using RNA-seq data revealed that *YAP1-1* mRNA expression was substantially lower than *YAP1-2* mRNA in both parental and PARPi-resistant cells. In addition, *YAP1-2γ* mRNA was the predominant *YAP1-2* splicing variant in parental cells (Supplementary Fig. 1g). However, in PARPi-resistant cells, *YAP1-2α* mRNA levels notably increased, while *YAP1-2β*, *YAP1-2γ*, and *YAP1-2δ* mRNA levels significantly decreased (Fig. 1d, e, Supplementary Fig. 1g). TCGA database analysis also showed that most human cancers predominantly express *YAP1-2γ* mRNA containing exons 5.2 and 6 (Supplementary Fig 1h). Thus, the predominant expression of *YAP1-2α* mRNA, a minor YAP1 splicing isoform in most cancer and normal cells, is a distinctive feature of PARPi-resistant cancer cells.

PARPi-resistant MDA-MB-436 and UBW1.289 cancer cells also resisted Cisplatin (Supplementary Fig. 1c, d). Similarly, Cisplatin-resistant UWB1.289 cells exhibited altered *YAP1* pre-mRNA splicing patterns (Fig. 1f). The resistance of cancer cells to DNA-damaging agents like PARPi and Cisplatin correlated with a shift in *YAP1* pre-mRNA splicing from the YAP1-2γ-dominant to the YAP1-2α-dominant pattern. To determine if the YAP1-2α isoform contributes to this resistance, MDA-MB-436 and UWB1.289 cells stably expressing each of the YAP1-2 isoforms were created. Upon treatment with Olaparib or Cisplatin, only cells ectopically expressing YAP1-2α showed resistance (Fig 1g). These results indicate that increased expression of the YAP1-2α isoform is linked to cancer cell resistance to genotoxic stress, such as PARPi or Cisplatin.

YAP1-2α induces LLPS in a splicing variation-dependent manner

To clarify the mechanism by which elevated levels of YAP1-2α contribute to drug resistance in cancer cells, we investigated the subcellular distribution of YAP1 in both parental and PARPi-resistant cells. Immunofluorescence staining of the parental cells, which predominantly expressed YAP1-2γ, revealed that YAP1 was broadly and uniformly distributed throughout the nucleus, except for the nucleoli. In contrast, in the PARPi-resistant cells that primarily expressed YAP1-2α, YAP1 immunofluorescence staining demonstrated the formation of punctate structures within the nucleus (Fig. 2a, Supplementary Fig. 2a).

Administration of 1,6-hexanediol (Hex), an agent that disrupts liquid-like condensates without affecting solid aggregates, to PARPi-resistant cells eliminated puncta formation. YAP1-2α-associated puncta formation was also observed in Cisplatin-resistant UWB1.289 cells (Supplementary Fig. 2b). We also generated *YAP1*-knockout (KO) UWB1.289 cells utilizing the CRISPR-Cas9 system. Immunoblot analysis confirmed the absence of endogenous YAP1-1 and YAP1-2 isoforms in the *YAP1*-KO cells (Fig. 2b, lane 2). These *YAP1*-KO cells were subsequently transfected with an expression vector for one of the four YAP1-2 isoforms fused with mVenus. The expression levels of the mVenus-fused YAP1-2 isoforms were comparable (Fig. 2b, lanes 3-6). We found nuclear puncta formation only in cells expressing mVenus-fused YAP1-2α (Fig. 2c, d, Supplementary Fig. 2c, d). To exclude the possibility that the puncta formation was due to the overexpression of mVenus-fused YAP1-2α, we also established *YAP1*-KO UWB1.289 cells reconstituted with HA-tagged YAP1-2α or YAP1-2γ at levels comparable to that of endogenous YAP1. Immunofluorescence analysis using an anti-YAP1 antibody revealed that nuclear YAP1 puncta were present in YAP1-2α-reconstituted cells but absent in YAP1-2γ-reconstituted cells (Fig. 2e). This finding indicates that YAP1-2α induces LLPS-mediated puncta formation in the nucleus. To further elucidate the membrane-less, liquid-like properties of the nuclear puncta induced by YAP1-2α, we conducted time-lapse imaging experiment and FRAP analysis in *YAP1*-KO UWB1.289 cells transfected with mVenus-fused

YAP1-2α. YAP1-2α was demonstrated to be responsible for membrane-less puncta formation (Fig. 2f-i Supplementary Fig. 2e-h). Based on these observations, we concluded that YAP1-2α is the only YAP1-2 splicing isoform capable of inducing LLPS in the nucleus.

LLPS is induced by YAP1-2α/TAZ complex formation

A previous study showed that the Leucine zipper in the coiled-coil region of YAP1-2α interacts with the Leucine zipper in TAZ's coiled-coil domain, forming a YAP1/TAZ heterodimer[32]. To determine if the Leucine zipper structure of YAP1-2α is crucial for LLPS-induced puncta formation, we created a YAP1-2α Leucine zipper mutant (LZM) by substituting the conserved Leucine residues with alanine, disrupting its structure. This disruption significantly reduced TEAD reporter activation by YAP1-2α (Supplementary Fig. 3a). Expressing mVenus-fused YAP1-2α(LZM) in *YAP1*-KO UWB1.289 or MDA-MB-436 cells markedly decreased puncta formation (Fig. 3a, b, Supplementary Fig. 3c). A proximity ligation assay (PLA) examined YAP1-2α and TAZ heterodimerization, revealing the YAP1-2α/TAZ complex in nuclear YAP1 puncta (Fig. 3b). TAZ also formed a heterodimer with YAP1-2α(S94A) but not with YAP1-2α(LZM), YAP1-2α(LZM|S94A), or YAP1-2γ in the nucleus (Supplementary Fig. 3d, upper). As expected, YAP1-2α, YAP1-2α(LZM), and YAP1-2γ interacted with TEAD, while YAP1-2α(S94A) and YAP1-2α(LZM|S94A) did not (Supplementary Fig. 3d, lower). Moreover, YAP1-2α-induced LLPS

puncta were eliminated by knocking out endogenous TAZ (Fig. 3c, Supplementary Fig. 3e) or by siRNA-mediated inhibition of TAZ expression (Supplementary Fig. 3f), confirming the essential role of TAZ in YAP1-2α-mediated LLPS induction.

To determine if TEAD (TEAD1-4), the critical YAP1-2α and TAZ partners, is necessary for LLPS-mediated nuclear puncta formation, we expressed mVenus-fused YAP1-2α (wild-type, LZM, S94A) and mVenus-fused YAP1-2γ in UWB1.289 cells. PLA (Fig. 3d, e) and immunofluorescence staining (Supplementary Fig. 3g) indicated a physical interaction between TEAD and wild-type YAP1-2α in nuclear puncta but not the LZM or S94A mutant. Moreover, K-975, a selective inhibitor of the interaction between TEAD and YAP1 or TAZ[37], eliminated LLPS puncta induced by YAP1-2α (Fig. 3f, Supplementary Fig. 3h). Thus, YAP1-2α-induced nuclear condensates contained YAP1-2α, TAZ, and TEAD complexes. In this regard, YAP1-2α(S94A) also formed small puncta independently of TEAD, albeit slightly (Fig. 3d, f), suggesting potential TEAD-independent mechanisms for weak condensate formation by YAP1-2α.

TAZ forms a homodimer via the Leucine zipper, leading to LLPS independently of YAP1 and TEAD[38]. In contrast, YAP1 cannot form homodimers. TAZ/TAZ-LLPS condensates were similarly produced in both parental and *YAP1*-KO cells (Supplementary Fig. 3i). PLA was used to visualize the interaction between TEAD and HA-tagged YAP1-2α or TAZ.

This technique allowed us to distinguish between YAP1-2α/TAZ-LLPS condensates and TAZ/TAZ-LLPS condensates (Supplementary Fig. 3j). Most YAP1-2α-TEAD complexes were localized within YAP1-2α/TAZ-induced LLPS condensates (Supplementary Fig. 3j, right), whereas TAZ-TEAD complexes were mainly outside TAZ/TAZ-induced LLPS condensates (Supplementary Fig. 3j, left). This indicates the indispensable role of TEAD in YAP1-2α/TAZ/TEAD-LLPS, while TAZ/TAZ-induced puncta likely contain other transcription factors. TAZ/TAZ homodimers were present in TAZ/TAZ-induced LLPS but absent in YAP1-2α/TAZ-LLPS (Supplementary Fig. 3k). These findings demonstrate that YAP1-2α/TAZ/TEAD-LLPS is distinct from TAZ/TAZ-LLPS, the former being formed by YAP1-2α, TAZ, and TEAD complex (YAP1-2α/TAZ/TEAD-LLPS), and the latter by TAZ homodimerization independent of YAP1 and TEAD (TAZ/TAZ-LLPS).

Mechanism of LLPS induction by YAP1/TAZ/TEAD complex formation

YAP1-1 mRNA expression is significantly lower than *YAP1-2* mRNA in various cell types, especially cancer cells[39]. In MDA-MB-436 cells, *YAP1-1α* mRNA expression is about ten times lower than *YAP1-2α* mRNA (Supplementary Fig. 1g). The YAP1-1α isoform possesses a single WW domain and a functional Leucine zipper in its coiled-coil region, allowing it to heterodimerize with TAZ via the Leucine zipper (Supplementary Fig. 4a). To investigate if YAP1-1α induces LLPS, we expressed YAP1-1α or

YAP1-2α in MDA-MB-436 cells. YAP1-1α produced fewer nuclear puncta than YAP1-2α, indicating it is significantly less effective in promoting LLPS induction (Fig. 4a, Supplementary Fig. 4b).

The WW domain is a protein motif that preferentially interacts with proline-containing sequences such as PPxY and LPxY motifs[36,40]. LLPS enables the formation of membrane-less puncta or droplets, where specific proteins are concentrated through multivalent interactions[41]. Nuclear puncta/condensates formed via LLPS, including transcription factors, co-activators, and mediators like BRD4 and MED1, are linked to super-enhancer formation. Thus, the presence of BRD4 in nuclear LLPS condensates indicates super-enhancers[42]. Mediators are crucial in various transcription aspects, including linking transcription factors to RNA polymerase II (Pol II)[43]. The role of BRD4 in LLPS relies on two bromodomains binding to H3K27ac, a marker of active enhancers[44]. Using PLA, we visualized BRD4 and H3K27ac interactions, identifying the BRD4/H3K27ac complex within YAP1-2α/TAZ/TEAD-induced LLPS condensates (Supplementary Fig. 4c). These findings suggest that YAP1-2α/TAZ/TEAD-induced LLPS causes the activation of a super-enhancer. Since BRD4 contains an LPxY motif (LPDY) in bromodomain I and a PPxY motif (PPTY) in its C-terminal proline-rich region (Fig. 4b), we hypothesized these motifs interact with the two WW domains of YAP1-2α to facilitate multivalent protein interactions. Protein-protein interaction modeling using AlphaFold2 predicted that YAP1-2α's WW domains (WW1

and WW2) interact with BRD4's PPxY and LPxY motifs (Fig. 4c, Supplementary Fig. 4d). Co-immunoprecipitation confirmed YAP1-2α and BRD4 interaction. This interaction was weakened when either PPxY or LPxY motif in BRD4 was disrupted and abolished when both were disrupted (Fig. 4d). Similar results were observed using PLA (Supplementary Fig. 4e). The significance of BRD4 in YAP1-2α/TAZ/TEAD-LLPS condensates was verified by the results that shRNA-mediated BRD4 knockdown and inhibition of YAP1-BRD4 interaction abolished puncta formation (Fig. 4e, Supplementary Fig. 4f, g). The reduction in YAP1-2α/TAZ/TEAD-LLPS puncta due to BRD4 knockdown was rescued by ectopic expression of shRNA-resistant wild-type BRD4, but not by BRD4 lacking one or both PPxY/LPxY motifs (Fig. 4f, Supplementary Fig. 4h). These findings indicate that BRD4's WW domains are crucial for generating YAP1-2α/TAZ/TEAD-induced LLPS condensates.

Activation of the YAP1-2α/TAZ/TEAD super-enhancer correlates with stem-like malignant properties in cancer cells

To evaluate the impact of YAP1-2α/TAZ/TEAD super-enhancer activation on gene expression, we stably expressed YAP1-2α or YAP1-2γ in MDA-MB-436 cells utilizing a lentiviral infection system. RNA-seq analysis revealed that elevated YAP1-2α expression resulted in the upregulation of 2,006 genes. In contrast, elevated YAP1-2γ expression, which does not

induce super-enhancers, led to the upregulation of 3,690 genes compared to controls (Supplementary Fig. 5a). Hallmark gene set analysis revealed distinct signatures for genes upregulated by YAP1-2α and YAP1-2γ (Supplementary Fig. 5b). Subsequently, we investigated the contribution of the YAP1-2α/TAZ/TEAD super-enhancer to the transcriptomic alterations induced by shRNA-mediated knockdown of BRD4, which is essential for super-enhancer activation[42,44,45]. BRD4 knockdown reduced the expression of 932 out of the YAP1-2α-induced 2,006 genes (Fig. 5a, b), indicating that these genes are positively regulated by the YAP1-2α/TAZ/TEAD super-enhancer. We further analyzed genes upregulated in PARPi-resistant (Fig. 1a) or YAP1-2α-expressing MDA-MB-436 cells and identified 965 genes (Fig. 5c), of which 450 genes were dependent on the YAP1-2α/TAZ/TEAD super-enhancer (Fig. 5c, left). Hallmark gene set analysis indicated that the 450 genes were strongly associated with EMT (Fig. 5c right, Supplementary Fig. 5c, d), which plays a crucial role in acquiring cancer stem-like properties[46-48]. The YAP1-2α/TAZ/TEAD super-enhancer may enhance the resilience of cancer cells by potentiating cancer stem-like malignant properties via EMT. Correspondingly, splice variant analysis of PARPi-resistant cancer cells revealed increased expression of CD44 variant isoforms (CD44v), including CD44v9 (Fig. 1d, Supplementary Fig. 5e), which are indicators of epithelial cancer stem-like populations[49,50]. These findings support the correlation between elevated YAP1-2α levels and cancer stem-like characteristics. Cell

populations exhibiting high levels of CD44v expression were isolated from MDA-MB-436 and UWB1.289 cells utilizing magnetic beads conjugated with an anti-CD44v9 antibody. Although the proportion of CD44v^{high} cells was low, they were present in both MDA-MB-436 and UWB1.289 cells (Fig. 5d). The CD44v^{high} cells demonstrated elevated levels of CD44v and YAP1-2α isoforms at both mRNA and protein levels (Fig. 5e, f). These CD44v^{high} cells also exhibited activation of genes regulated by the YAP1-2α/TAZ/TEAD super-enhancer, as evidenced by *POLQ* encoding DNA polymerase theta (POLQ), which confers resistance to PARPi in *BRCA*-deficient cancer cells through activation of the microhomology-mediated end-joining (MMEJ) repair pathway[51,52] and *ALDH1A*, a marker of cancer stem-like cells (Fig. 5b, g)[53]. The elevated expression of these genes was inhibited by treatment with JQ1 (Fig. 5g), the selective inhibitor of BRD4-regulated super-enhancers[54]. CD44v^{high} cells also exhibited YAP1-2α puncta formation, which were eliminated by JQ1, indicating the activation of the YAP1-2α/TAZ/TEAD super-enhancer in the cells (Supplementary Fig. 5f). These findings suggest that activation of the YAP1-2α/TAZ/TEAD super-enhancer restructures the transcriptional network to promote the acquisition of cancer stem-like properties, thereby increasing the robustness and resilience of cancer cells against various adverse conditions.

Mechanisms by which induction of the YAP1-2α/TAZ/TEAD super-

enhancer endows resistance to genotoxic agents

The YAP1-2α/TAZ/TEAD super-enhancer significantly upregulated POLQ, a druggable target in PARPi-resistant *BRCA*-deficient cancers (Fig. 5b)[52]. To investigate whether the POLQ-MMEJ pathway contributes to resistance to PARPi and Cisplatin, we evaluated the sensitivity of YAP1-2α-overexpressing, PARPi-resistant, or CD44v^{high} *BRCA*-deficient cancer cells to Olaparib or Cisplatin. The suppression of POLQ expression in these cells significantly reduced MMEJ activity to the level of parental cells (Fig. 6a-c, Supplementary Fig. 6a-c). In contrast, POLQ inhibition only partially restored sensitivity to Olaparib or Cisplatin (Fig. 6d-f, Supplementary Fig. 6d). YAP1-2α(LZM), which does not activate the YAP1-2α/TAZ/TEAD super-enhancer, did not induce PARPi resistance (Supplementary Fig. 6e). Therefore, pathways or mechanisms other than the POLQ-MMEJ axis may also exist through which the YAP1-2α/TAZ/TEAD super-enhancer confers PARPi/Cisplatin resistance. Indeed, the super-enhancer regulates genes associated with the acquisition of cancer stem-like properties that enhance drug resistance[46-48,53]. Three-dimensional (3D) cell culture is generally considered superior to two-dimensional (2D) culture for analyzing cancer stem-like properties, as it provides a more physiologically relevant microenvironment that more accurately replicates the *in vivo* conditions of tumors[55]. 3D cultures frequently exhibit different drug sensitivities compared to 2D cultures, which may more accurately predict *in vivo* responses[56]. Consequently, we re-examined the role of the POLQ-MMEJ axis in PARPi resistance

utilizing 3D-cultured spheroids prepared from CD44v^{high} *BRCA*-deficient cancer cells. As observed in 2D cultures, spheroids derived from CD44v^{high} cells demonstrated increased resistance to PARPi and Cisplatin compared to spheroids derived from parental or CD44v^{low} cells (Supplementary Fig. 6f). However, the inhibition of POLQ in CD44v^{high} spheroids only partially restored drug sensitivity (Supplementary Fig. 6g), suggesting again that the induction of POLQ by the YAP1-2α/TAZ/TEAD super-enhancer does not fully account for the acquisition of resistance to PARPi/Cisplatin in *BRCA*-deficient cancer cells. In contrast, inhibition of the super-enhancer almost fully restored the cell sensitivity to PARPi/Cisplatin (Fig. 6g, Supplementary Fig. 6h). Furthermore, sphere-forming activity was enhanced in CD44v^{high} spheroids, which was abolished by inhibiting the formation of the YAP1-2α/TAZ/TEAD super-enhancer (Fig. 6h-k, Supplementary Fig. 6h-j), confirming that YAP1-2α/TAZ/TEAD super-enhancer activation conferred cancer stem-like properties. These findings indicated that the acquisition of resistance in *BRCA*-deficient cancer cells to Olaparib and Cisplatin results from the combined effects of cancer stem-like resilience and POLQ, both of which are induced by activation of the YAP1-2α/TAZ/TEAD super-enhancer.

Resistance to anticancer drugs correlates with elevated malignant grades of cancer cells

The aforementioned results indicated that the increased drug resistance encompasses enhanced cancer stem-like properties characterized by

augmented robustness of malignant phenotypes[57]. Accordingly, we investigated the cancer stem-like properties in YAP1-2α-overexpressing or PARPi-resistant UWB1.289 cells. In 3D culture, these cells demonstrated significantly enhanced sphere-forming activity compared to their parental cells, which was abolished by K-975 or JQ1 treatment (Fig. 7a, Supplementary Fig. 7a). YAP1-2α-expressing cells and PARPi-resistant cells also exhibited aggressive characteristics, including enhanced anchorage-independent growth, higher ferroptosis resistance, increased motility, and elevated invasiveness into the extracellular matrix (Fig. 7b, c, d, e, Supplementary Fig. 7b, c). They also resisted various anticancer agents, including molecular targeted drugs (Supplementary Fig. 7d). These characteristics are attributable to the activated YAP1-2α/TAZ/TEAD super-enhancer, suggesting that its activation in cancer cells under challenging conditions confers a more aggressive and malignant phenotype compared to their parental cells.

We also analyzed clinical cancer specimens to investigate the enhanced malignant properties of cancer cells. Ovarian cancer tissues exhibiting elevated *YAP1-2α* expression were associated with increased POLQ expression and more advanced clinical grades (Fig. 7f-i, Supplementary Fig. 7e-g). Moreover, in accordance with the *in vitro* findings, tumor regions exhibiting elevated levels of *YAP1-2α* and POLQ expression demonstrated correspondingly higher CD44v expression (Fig. 7g, bottom). Analysis of the TCGA dataset further revealed that patients exhibiting higher expression levels of *YAP1* mRNA excluding exon 6 and

higher expression levels of *CD44v* mRNA demonstrated significantly poorer prognoses compared to those with lower expression levels of *YAP1* mRNA including exon 6 and lower expression levels of *CD44v* mRNA (Fig. 7j, Supplementary Fig. 7h) in both ovarian (OV) and triple-negative breast cancer (TNBC). Consequently, ovarian cancers and TNBCs classified as $CD44v^{high}/YAP1\text{-}2\alpha^{high}$ are associated with poor clinical outcomes, attributable, at least in part, to the activation of the YAP1-2α/TAZ/TEAD super-enhancer, which increases malignant grades of cancer cells.

To assess the *in vivo* relevance of YAP1-2α/TAZ/TEAD super-enhancer formation, a tumor xenograft assay was conducted utilizing MKN45 human gastric epithelial cells. Subcutaneous inoculation of MKN45 cells ectopically overexpressing YAP1-2α resulted in significantly larger tumors than parental MKN45 cells in nude mice. In contrast, MKN45 cells ectopically expressing mutant YAP1-2α(LZM), which cannot interact with TAZ, exhibited tumor formation comparable to that of parental cells (Fig. 7k, Supplementary Fig. 7i). These findings indicated that YAP1-2α/TAZ/TEAD super-enhancer activation enhances the *in vivo* tumorigenicity of cancer cells.

Discussion

This study demonstrated that prolonged exposure of *BRCA*-deficient cancer cells to genotoxic agents, such as PARPi and Cisplatin, induces the activation of a super-enhancer that potentiates cancer stem-like characteristics with increased malignancy that contributes to therapeutic resistance. The formation of this super-enhancer is initiated by the upregulation of YAP1-2α, a minor isoform of YAP1 that distinctively possesses a Leucine zipper dimerization motif, upon prolonged exposure to PARPi/Cisplatin. Elevated YAP1-2α levels are inversely correlated with reduced levels of major YAP1 isoforms, YAP1-2γ and YAP1-2δ, indicating a shift in the *YAP1* pre-mRNA splicing pattern during the acquisition of drug resistance. Upregulated YAP1-2α heterodimerizes with TAZ via the Leucine zipper without affecting YAP1-2α-TEAD and TAZ-TEAD complex formation. The association of YAP1-2α-TEAD and TAZ-TEAD through the YAP1-2α/TAZ interaction induces LLPS-mediated nuclear condensates, which activate the YAP1-2α/TAZ/TEAD super-enhancer via multivalent interactions between YAP1-2α, TAZ, and BRD4. YAP1-1α can also heterodimerize with TAZ through the Leucine zipper. However, YAP1-1α infrequently induces puncta formation, presumably due to its single WW domain limiting multivalent protein interactions necessary for LLPS (YAP1-2α possesses two WW domains). Independent of YAP1 and TEAD, TAZ promotes LLPS-mediated puncta formation through Leucine zipper-mediated homodimerization. In contrast to TAZ, YAP1-1α and

YAP1-2α cannot homodimerize or heterodimerize owing to the structural incompatibilities between the identical Leucine zipper sequences[32,38]. TAZ is, therefore, associated with a minimum of two distinct super-enhancers: one involving the YAP1-2α/TAZ heterodimer and the other involving the TAZ homodimer, each regulating different sets of target genes.

YAP1 and TAZ regulate numerous genes, including those involved in cell proliferation, cell-cell contact, cell polarity, cellular stress, cell metabolism, and cell cycle[21-27]. Despite their redundant roles in gene regulation, as their primary partner transcription factors are TEADs (TEAD1-4), most studies have suggested that the YAP1-TEAD and TAZ-TEAD transcriptional complexes function independently[29,58]. Eight YAP1 isoforms are generated in human cells by differential splicing of *YAP1* pre-mRNA[31,32,35]. Among these, YAP1-2γ and YAP1-2δ, which lack a functional Leucine zipper, are predominantly expressed in both normal and cancer cells. Consequently, our understanding of the YAP1/TAZ heterodimer remained limited until the discovery that YAP1-1α and YAP1-2α are the sole YAP1 isoforms capable of binding TAZ through Leucine zippers[34]. The present study further revealed that YAP1-2α/TAZ heterodimerization activates a super-enhancer comprising YAP1-2α, TAZ, TEAD, and BRD4, which significantly contributed to the acquisition of PARPi/Cisplatin resistance in *BRCA*-deficient cancer cells. Activation of DNA polymerase theta (POLQ), a unique DNA polymerase that is essential for microhomology-mediated end-joining (MMEJ)[51,52], promotes error-

prone repair of double-strand breaks (DSBs) induced by DNA-damaging agents in *BRCA*-deficient cells. This error-prone process also increases the probability of reverse- or second-site mutations in mutated driver genes[59]. However, the induction of POLQ by the super-enhancer cannot fully explain the acquisition of *BRCA*-deficient cell resistance to PARPi/Cisplatin, as the inhibition of POLQ expression only partially restored drug sensitivity, whereas disruption of the YAP1-2α/TAZ/TEAD super-enhancer almost completely abolished drug resistance.

What mechanism underlies the activation of the YAP1-2α/TAZ/TEAD enhancer in conferring substantial resistance to *BRCA*-deficient cells beyond the induction of POLQ? A potential explanation arises from the observation that PARPi/Cisplatin-resistant *BRCA*-deficient cancer cells with active YAP1-2α/TAZ/TEAD super-enhancers also exhibit elevated levels of *CD44* splicing variants (*CD44v*), which are indicators of cancer stem-like cells[60]. The super-enhancer may reconfigure transcriptional networks to potentiate cancer stem-like properties, such as increased self-renewal capacity (3D spheroid formation), enhanced motility and invasion, and elevated resistance to pro-apoptotic signaling. This phenomenon strengthens the malignant characteristics of cancer cells and enhances their resilience to various adverse stresses and conditions. We believe that the activation of YAP1-2α/TAZ/TEAD super-enhancers may not be specific to *BRCA*-deficient cancer cells exposed to genotoxic stress. Instead, cancer cells subjected to adverse conditions may selectively expand CD44v^{high}/YAP1-2α^{high} cancer stem-like cells, which typically

exist at low frequencies within the cancer cell population, or actively modulate the splicing mechanism of *YAP1* pre-mRNA from a "*YAP1-2γ/δ*-dominant" to a "*YAP1-2α*-dominant" pattern to cope with challenging conditions in a general manner. Consistent with this notion, *BRCA*-deficient cancer cells exhibiting the activated YAP1-2α/TAZ/TEAD super-enhancer also demonstrated increased resistance to the MEK inhibitor Trametinib and the multi-kinase inhibitor Sorafenib, suggesting that the acquisition of resistance to anticancer drugs (including molecular targeted drugs) in *BRCA*-deficient cancers is not limited to DNA-damaging agents.

The YAP1-2α/TAZ/TEAD super-enhancer activates cytokines and chemokines, thereby promoting the polarization and recruitment of myeloid-derived suppressor cells (MDSCs) and tumor-associated macrophages (TAMs), which subsequently inactivate T cells[61,62]. Interferon-γ-induced YAP1 phase separation activates PD-L1[63], potentially triggering the YAP1-2α/TAZ/TEAD super-enhancer and facilitating immune evasion by cancer cells. YAP1-directed super-enhancers augment cell-intrinsic robustness and facilitate cell-extrinsic conditions that foster cancer cells, establishing a "cold" immune environment and thereby contributing to the malignant progression of cancer.

The present study elucidated an unanticipated molecular connection between alternative mRNA splicing, liquid-liquid phase separation (LLPS), and super-enhancers, which significantly alters cancer cell characteristics

without genetic mutations. Recent studies have demonstrated a robust correlation between aberrant alternative splicing and cancer[64]. The findings of the present study provide valuable insights into the mechanisms by which splicing abnormalities contribute to the progression of cancer. Activating YAP1-2α/TAZ/TEAD super-enhancers in cancer cells under adverse stresses/conditions confers a more aggressive and malignant phenotype than their parental cells, enabling them to overcome challenging environments. Selective inhibition of differential splicing that generates *YAP1-2α* mRNA impedes cancer progression and mitigates resistance to anticancer therapies.

Methods

Cell Lines

UWB1.289 cells (ATCC, CRL-2945) were cultured in 1:1 mixed medium supplemented with 3% FBS (Gibco), a 1:1 mixture of mammary epithelial cell growth medium (MEGM) (Lonza, CC-3150) without GA-1000 (gentamicin-amphotericin B mixture) and RPMI-1640 (Wako, 189-02025) supplemented with 10 mM HEPES and 1 mM sodium pyruvate. MDA-MB-436 (ATCC, HTB-130) and MKN45 (JCRB Cell Bank, JCRB0254) cells were cultured in RPMI-1640 supplemented with 10% FBS (Gibco), 10 mM HEPES, and 1 mM sodium pyruvate. Lenti-X 293T cells (Clontech Laboratories, 632180) were cultured in D-MEM (Wako, 044-29765) supplemented with 10% FBS (Gibco) and 1 mM sodium pyruvate. Cells were incubated at 37 °C in 5% CO_2.

To generate gene knockout (KO) cell lines, cells were transfected with pX330-sgYAP1 or pX330-sgTAZ vector and a selection vector containing the blasticidin S resistance gene. After transfection, the cells were selected using blasticidin S (10 μg/ml) and cloned by limiting dilution. To establish PARPi-resistant cell clones, cells were treated with 100 nM olaparib (MedChemExpress, HY-10162) for one week, and the surviving cells were cultured and expanded. The expanded cells were further treated with 1 μM Olaparib for one week and then expanded. After Olaparib administration, cells were subcloned using the limiting dilution method. Cisplatin-resistant clones were established from UWB1.289 cells after three months of cell culture with stepwise increases (100 pM to 1000 nM) in Cisplatin (MedChemExpress, HY-17394) concentration. $CD44v^{high}$ and $CD44v^{low}$ cells were collected from UWB1.289 or MDA-MB-436 cells using a Magnetic Cell separation kit (COSMO Bio, CSC-SEP1). Mycoplasma contamination in the cell culture was examined. There was no sign of mycoplasma contamination in the cell lines used in this study. See our previous work for the method details[65].

Three-Dimensional Overlay Culture

UWB1.289 cells were suspended in 1:1 mixed medium containing 2% Matrigel (CORNING, #356231) (termed assay medium) and seeded onto Matrigel in 8-well chamber slides at 4×10^3 cells/well. Eight days after seeding, the spheroids were treated with 100 nM JQ1 (MedChemExpress, HY-13030), 1 μM K-975 (MedChemExpress, HY-138565), or DMSO as a mock control for 6 days. During cultivation, the assay medium with or without the indicated reagent was replaced every two days. After treatment with the appropriate reagents, spheroids were fixed with 2% paraformaldehyde for 20 min and collected using a cell-recovery solution (CORNING, 354253). The fixed spheroids were permeabilized with 0.5% TritonX-100 in PBS for 20 min at room temperature and subjected to immunostaining analysis. The Ferret diameters of spheroids were determined by measuring images taken 14 days after seeding using the ImageJ software.

Expression Vectors

The expression vectors used in this study are shown in supplementary table 2. Base substitution and deletion mutants were generated using a KOD-plus-Mutagenesis kit according to the manufacturer's instructions (TOYOBO, SMK-101). Nucleotide sequences of all constructed vectors were confirmed by Sanger sequencing.

Preparation of Lentivirus and Infections

The lentivirus was produced according to our previous protocol[65].

Detection for Splicing Isoforms

Total RNA was extracted from the cells using TRIzol reagent (Invitrogen, 15596026) and subjected to reverse transcription using oligo-dT primers and SuperScript II Reverse Transcriptase (Invitrogen, 18064014). The generated cDNA was subjected to PCR to detect the *YAP1* exon 6 sequence,

which encodes the γ-segment, or *CD44* splice variants. After PCR, the amplicon was applied to 0.8% (for *CD44* splice variants) or 2% (for *YAP1* exon 6) TAE-agarose gel, and electrophoresis was performed.

Live Cell Imaging

Cells transfected with mVenus-fused YAP1 isoforms were subjected to analysis to confirm the liquid-like properties (fusion event of puncta, disruption of puncta formation by treatment with Hex and FRAP). To detect the fusion event of the YAP1-2α puncta, time-lapse fluorescence images of cells transfected with mVenus-fused YAP1-2α were obtained for 120 s using a FLUOVIEW FV1200 confocal microscope (Olympus). To observe the disruption of YAP1-2α puncta formation by Hex treatment, transfected cells were treated with 1% Hex for 20 min. Twenty minutes after Hex treatment, the cells were washed and incubated for another 4 h. Fluorescence signals were detected at the indicated time points.

Fluorescence Recovery After Photobleaching (FRAP)

The mVenus-fused YAP1-2α nuclear puncta specified by the ROI were photobleached by laser irradiation. After photobleaching, time-lapse fluorescence images of the YAP1-2α puncta were obtained for 120 sec. Unbleached puncta were used as controls. The images were acquired at 3.2 second intervals using a 40x objective lens. The fluorescence intensities of puncta obtained from a series of time-lapse images were analyzed using FLUOVIEW FV1200 software.

Immunofluorescence Staining

Cells were fixed with 4% paraformaldehyde in PBS for 15 min at room temperature, permeabilized with 0.25% TritonX-100 in PBS for 10 min at room temperature, and blocked in blocking solution (5% BSA, 0.1% Tween20, 0.05% NaN3 in PBS) for 60 min at room temperature. For spheroid staining, fixed and collected spheroids were permeabilized with

0.5% TritonX-100 in PBS for 20 min at room temperature. Blocked cells/spheroids were incubated with primary antibodies against γ-H2AX (CST, 9718, 1:500), YAP1 (CST, 12395, 1:500 or CST, 14074, 1:500), HA-tag (CST, 2367, 1:500 or CST, 3724, 1:500), GFP (MBL, 598, 1:500), TAZ (CST, 83669, 1:500), pan-TEAD (CST, 13295, 1:500), Flag-tag (SIGMA, F3165, 1:1000), BRD4 (CST, 13440, 1:500), H3K27ac (CST, 8173, 1:500), CD44v9 (COSMO Bio, LKG-M001, 1:200) or ki67 (Thermo Fisher Scientific, 14-5698-80, 1:500). After the antigen-antibody reaction, Alexa Fluor-conjugated secondary antibodies (1:1000) and/or Alexa Fluor-conjugated phalloidin (Invitrogen) were used. Nuclei were stained with DAPI (wako, 043-18804, 1:1000) solution.

Proximity Ligation Assay

PLA was performed using a Duolink *In situ* PLA kit (SIGMA, Duo92007, Duo92002, Duo92004) according to the manufacturer's instructions. PL spots were counted using ImageJ software and analyzed using PRISM GraphPad software. For more details on PLA analysis, see our published protocol[65].

Immunohistochemistry

The human ovarian cancer tissue array (OV0071a, OV1004A, US Biomax) was deparaffinised and rehydrated. Antigen retrieval was performed by boiling for 15 minutes in 1x Target Retrieval (ACD). To block endogenous peroxidase activity, the tissue array was incubated with 3% hydrogen peroxide in double-distilled water for 10 min at room temperature. The array was then incubated overnight at 4 °C with a primary antibody against POLQ (MyBioSource, MBS9612322, 1:200) or CD44v9 (COSMO Bio, LKG-M001, 1:200). After the antigen-antibody reaction, the array was incubated for 60 min at room temperature with Alexa Fluor-conjugated secondary antibodies (1:1000). After the secondary antibody reaction, the nuclei were stained with DAPI solution (1:1000) for 20 min at room temperature. Fluorescence images were obtained using FLUOVIEW

FV1200 confocal microscope. H&E staining was performed using the Hematoxylin and Eosin Stain kit (ScyTek Laboratories).

In Situ Hybridization (BaseScope)

Deparaffinized and rehydrated tissue arrays were subjected to *in situ* hybridization (BaseScope). BaseScope was performed using the BaseScope Detection Reagent Kit v2-RED (ACD) according to the manufacturer's instructions. After sequential BaseScope reactions, immunofluorescence staining with anti-CD44v9 or anti-POLQ antibody was performed. The human YAP1-1/2α-isoform-specific probe (BA-Hs-YAP1-tv3-E5E6) was designed using an ACD. The expression levels of POLQ protein and *YAP1-2α* mRNA were determined by measuring the POLQ immunofluorescence intensity and *YAP1-2α* mRNA BaseScope signals using the ImageJ software. *YAP1-2α* mRNA expression was scored as 0: no staining or less than 1 dot to every 20 cells; 1+: 1 dot/cell; 2+: 2-3 dots/cell, no or very few dot clusters; 3+: 4-10 dots/cell, less than 10% positive cells have dot clusters; 4+: >10 dots/cell, more than 10% positive cells have dot clusters. Staining scores were set according to the scoring guidelines of BaseScope.

Immunoprecipitation and Immunoblotting

The cells were washed in ice-cold PBS and lysed in RIPA buffer (CST, 9806). For immunoprecipitation, the washed cells were lysed in lysis buffer (100 mM NaCl, 50 mM Tris-HCl pH 7.5, 5 mM EDTA, 2 mM Na_3VO_4, 10 mM NaF, 10 mM β-glycerophosphate, 2 mM PMSF, 10 μg/ml leupeptin, 10 μg/ml trypsin inhibitor, 10 μg/ml aprotinin, and 0.5% NP-40) and sonicated. Cell lysates were incubated with protein G-beads after incubation with anti-TAZ or anti-Flag antibody. The beads were washed five times with lysis buffer, and the immunoprecipitates were eluted using SDS sample buffer. The immunoprecipitates and total cell lysates were subjected to SDS-PAGE, followed by immunoblotting. To compare protein

expression levels, protein band intensities obtained from three biological replicate experiments were collected and quantitatively analyzed using LAS-4000 imager (FUJIFILM).

Quantitative PCR (qPCR)

Total RNA was extracted from cells or spheroids using TRIzol reagent (Invitrogen) and reverse-transcribed using the High-Capacity cDNA Reverse Transcription Kit (Thermo Fisher Scientific, 4368814). Relative mRNA expression was analyzed using the QuantStudio 3 Real-Time PCR System (Thermo Fisher Scientific) with SYBR *Premix Ex Taq* Tli RNaseH Plus (TaKaRa). *18S* rRNA was used as an internal control. The data were analyzed using the comparative CT (ΔΔCT) method.

Luciferase Reporter Assay

A luciferase reporter assay was performed using a dual luciferase reporter assay kit (Promega, E1960). See our previous work for details.[65] To examine the effect of YAP1-2α mutants on TEAD activity, *YAP1*-KO UWB1.289 cells were transfected with the TEAD reporter plasmid together with the indicated mVenus-fused YAP1-2α mutant expression vector (wild-type, LZM, S94A, LZM|S94A) using Lipofectamine 2000 reagent (Invitrogen), and 48 h after transfection, cells were collected using passive lysis buffer (Promega). Luminescence was detected using a Centro XS^3 LB960 (BERTHOLD). The relative luciferase activities were calculated as fold changes relative to the values of the control samples. To confirm the protein expression levels of the mVenus-fused YAP1-2α mutants, the remaining cell lysates were subjected to immunoblotting.

MMEJ Reporter Assay

Plasmid containing the MMEJ reporter cassettes (EJ2GFP-puro, Addgene: #44025) was linearized by *I-SceI* and then introduced into cells by transfection using Lipofectamine 2000. Transfected cells were selected by

treatment with 1 μg/ml puromycin for three days. After puromycin selection, the number of GFP-positive cells and total cells were determined using an automatic cell counter Countess 3 FL (Invitrogen). The efficiency of DNA repair was determined by calculating the ratio of GFP-positive cells to the total cells.

Cell Viability Assay

Sensitivity to anti-cancer agents was measured by MTS assay using CellTiter 96 AQueous One Solution Cell Proliferation Assay (Promega, G3580) according to the manufacturer's instructions. To examine drug sensitivity, 1,000 cells were seeded into each well of 96-well plates and treated with stepwise concentrations of anticancer agents (Cisplatin, Sorafenib, Staurosporine, Taxol, Trametinib) for 72 h. To examine sensitivity to PARPi, 500 cells were seeded into each well of 96-well plates and treated with a stepwise concentration of olaparib for 6 days. After treatment with anti-cancer agents, the cells were incubated with the MTS assay reagent at 37 °C in 5% CO_2. After 60-90 min of incubation, the absorbance at 490 nm was measured using Multiskan FC (Thermo Fisher Scientific). The relative cell viability was calculated using mock-treated cells.

Three-dimensional Cell Viability Assay

Spheroids cultured in three dimensions were subjected to a cell growth assay or a drug sensitivity assay. For the cell growth assay, cultured spheroids were treated with 100 nM JQ1 or DMSO as a mock control for 6 days. To examine gene expression levels, spheroids treated with each reagent for 3 days were collected and subjected to qPCR analysis. For the drug sensitivity assay, cells were seeded at 500 cells per well onto Matrigel in 8-well chamber slides and cultured until they became spheroids. The spheroids were treated with stepwise concentrations of Olaparib or Cisplatin along with 100 nM JQ1, 1 μM K-975, or DMSO as

mock control for 10 (for Olaparib) or 6 (for Cisplatin) days, respectively. Specifically, to examine anchorage-independent growth, cells were seeded at 1,000 cells per well into an Ultra-Low Attachment 6-well plate (CORNING) and cultured for 8 days until the cells became spheroids. The spheroids were treated with 100 nM of JQ1, 1 μM of K-975 or DMSO as mock control for 6 days. During cultivation, the medium with or without the indicated reagents was replaced every 2 days. Appropriately cultured spheroids were lysed in CellTiter-Glo 3D Cell Viability Assay Reagent (Promega, G9683). The 200 μl cell lysate obtained from each well was immediately transferred into a white 96-well plate (Greiner) and luminescence was measured using Centro XS^3 LB960. To ensure linearity of the luminescence signal in these assays, dilution operations were performed as appropriate. Relative cell growth and viability were calculated using mock-treated cells.

Ferroptosis Assay

Cells treated with 100 nM JQ1, 1 μM K-975, or DMSO as a mock control for 3 days were seeded into a 96-well plate (Greiner) or clear-bottom/black 96-well plate (FALCON) and further treated with chlorido [N, N'-Disalicylidene-1,2-Phenylenediamine] Iron (III) (Cayman Chemical Company, 28788) or DMSO as a mock control for 48 h (to examine ferroptosis) or 24 h (to examine lipid hydroperoxide), respectively. Specifically, to examine the effect of GPX4 on resistance to ferroptosis, cells were treated with chlorido [N, N'-Disalicylidene-1,2-Phenylenediamine] iron (III) together with a stepwise concentration of GPX4 inhibitor ML-210 (Selleck, S0788) for 48 h. Appropriately cultured cells were lysed in CellTiter-Glo 3D Cell Viability Assay reagents (Promega). Cell viability was determined by detecting luminescence using a Centro XS3 LB960. To examine lipid hydroperoxide (LPO), appropriately cultured cells were incubated with the lipid peroxidation probe BDP 581/591 C11- (DOJINDO, L267) at 37 °C in 5% CO2 according

to the manufacture's protocol. After 30 min of incubation, the fluorescence (excitation: 540 nm, emission: 580 nm) was measured using a Nivo Multimode microplate reader (PerkinElmer). The number of surviving cells was determined by detecting luminescence using the CellTiter-Glo 3D Cell Viability Assay (Promega). To determine lipid hydroperoxide (LPO) per cell, LPO/cell was calculated as LPO fluorescence intensity per well/cell number per well (intensity of luminescence).

Migration and Invasion Assay

Cells treated with 100 nM JQ1, 1 μM K-975, or DMSO as a mock control for 3 days were seeded into Transwell plates (Costar: 3464) inserted into 24-well plates (Coater: 3526). Transwell coated with type-I-A collagen gel (Wako), prepared according to the manufacturer's protocols, was used to examine the ability of the cells to infiltrate the extracellular matrix (invasion assay). The cells were further cultured in medium containing 0.1% FBS for 48 h (migration assay) or 2 weeks (invasion assay). The bottom wells were filled with medium containing 10% FBS. After incubation for the appropriate time, cells that had migrated or infiltrated into the lower wells were lysed in CellTiter-Glo 3D Cell Viability Assay regents. The cell number was determined by detecting luminescence using Centro XS3 LB960.

Prediction of Molecular Complex Structure

The complex structure of WW1 or WW2 domain of YAP1-2α with the BRD4 LPxY or PPxY motif was predicted using AlphaFold2 multimer via the Colabfold v1.5.5 web server (https://colab.research.google.com/github/sokrypton/ColabFold/blob/main/AlphaFold2.ipynb). The buried surface area of the LPxY or PPxY motifs in the complex was estimated using the PDBePISA web server (https://www.ebi.ac.uk/pdbe/pisa/). Structural graphics were generated using PyMOL v2.5.0.

Expression Correlation Analysis

Clinical and IHC data, *POLQ* mRNA expression data, expression data of *YAP1* mRNA splicing variants containing γ-segment (referred to as *YAP1-E6*), and expression data of *CD44v8-10* mRNA splicing variants (*CD44v*) in TCGA cohort (BRCA, OV) were downloaded directly from the cBioportal for Cancer Genomics (https://www.cbioportal.org/)[66-68] and TCGA SpliceSeq (https://bioinformatics.mdanderson.org/TCGASpliceSeq/singlegene.jsp) [69] Stratification of tumor subtypes (triple-negative breast cancer: TNBC) using IHC data was performed according to our previous study[65]. Expression correlations between *POLQ* and *YAP1-E6* or *CD44v* and *YAP1-E6* were determined by scatter plot analysis using Pearson's correlation coefficient.

Kaplan-Meier analysis

For subgrouping the TCGA cohorts, expression of *CD44v* or *YAP1-E6* was defined as "high" (PSI > 0.5 or PSI > 0.65) and "low" (PSI <0.5 or PSI < 0.65), respectively. TNBC and serous ovarian cancer patients (n = 169 and 197) were divided into the "$CD44v^{high}$ and $YAP1\text{-}E6^{low}$" (n =11 and n=24), "$CD44v^{high}$ and $YAP1\text{-}E6^{high}$" (n=71 and n=75), "$CD44v^{low}$ and $YAP1\text{-}E6^{low}$" (n=3 and n=7), and "$CD44v^{low}$ and $YAP1\text{-}E6^{high}$" (n=84 and n=91) groups, respectively. The overall survival of patients with "$CD44v^{high}$ and $YAP1\text{-}E6^{low}$" cancer versus patients with "$CD44v^{low}$ and $YAP1\text{-}E6^{high}$" cancer was analyzed by Kaplan-Meier survival curve analysis using PRISM GraphPad software.

RNA Sequencing and Splicing Variant Analysis

Total RNA was extracted from cells using ReliaPrep RNA Miniprep Systems (Promega) and purified using NEBNext Poly(A) mRNA Magnetic Isolation Module (NEB). RNA libraries for RNA-seq were prepared using NEBNext Ultra II Directional RNA Library Prep Kit (NEB). RNA sequencing was performed using Illumina NovaSeq 6000. For splicing

variant analysis, the differential usage of splice junctions and exons were determined using JunctionSeq (Version 3.6.1). Genes with elevated expression (adjusted $P < 0.05$) were subjected to gene ontology (GO) or hallmark gene set analysis. GO analysis and hallmark gene set analysis were performed using the GO analysis tool Metascape (https://metascape.org/gp/index.html#/main/step1)[70]. Specific gene sets (Fig. 1: Enrichment > 2.5, Log $P < -2$; Fig. 5: Enrichment > 4, Log $P < -3$) were selected and represented in bar graphs. To identify YAP1-2α LLPS-dependent genes, genes that were upregulated by YAP1-2α (adjusted $P < 0.05$) and downregulated by BRD4 inhibition (adjusted $P < 0.05$) were defined as YAP1-2α super-enhancer target genes.

Tumor Xenograft Assay

BALB/cAJcl-nu/nu female mice at five weeks of age were purchased from CLEA Japan and were used for xenograft assays. MKN45 cells that had been infected with an HA-tagged YAP1-2α (WT or LZM) expression lentivirus or a control lentivirus were selected using puromycin. Puromycin-resistant cells were suspended in PBS containing 50% Matrigel (CORNING, 356231) at 3×10^7 cells/ml and were injected into the flank of female nude mice by subcutaneous injection (3×10^6 cells /0.1 ml). The mice were maintained in a pathogen-free environment for 20 days. The tumor size was measured twice weekly using calipers. Tumor volume was calculated using the formula: V (mm^3) = larger diameter × (smaller diameter)^2 × 1/2. All animal experiments were performed in accordance with the protocol approved by the Ethics Committee for Animal Experiments of the Institute of Microbial Chemistry, Microbial Chemistry Research Foundation.

Statistics and reproducibility

The specific statistical methods used are indicated in the figure legends, and were calculated using Microsoft Excel and PRISM GraphPad software.

Unpaired t-tests or U-tests were performed to compare the two groups. Details of the analysis are provided in the respective methods. All experiments presented in the manuscript were repeated in at least two independent experiments, three technical or biological replicates.

Reporting summary

Further information on research design is available in the Nature Portfolio Reporting Summary linked to this article.

Data availability

Raw RNA sequencing data created in this study have been uploaded to the Gene Expression Omnibus (GEO; https://www.ncbi.nlm.nih.gov/geo/) and are available under accession code (GSE287274).

All the other data supporting the findings of this study are available within the article and its supplementary information files and source data. Source data are provided with this paper.

Code availability

This study did not generate the original code.

References

1. Lovly, C.M. & Shaw, A.T. Molecular pathways: resistance to kinase inhibitors and implications for therapeutic strategies. *Clin. Cancer Res.* **20**, 2249-2256 (2014). https://doi.org/10.1158/1078-0432.CCR-13-1610.
2. Panda, M. & Biswal, B.K. Cell signaling and cancer: a mechanistic insight into drug resistance. *Mol. Biol. Rep.* **46**, 5645-5659 (2019). https://doi.org/10.1007/s11033-019-04958-6.
3. Pepita Giménez-Bonafé, P., Tortosa, A. & Ricardo Pérez-Tomás, R. Overcoming drug resistance by enhancing apoptosis of tumor cells. *Curr. Cancer Drug Targets* **9**, 320-340 (2009). https://doi.org/10.2174/156800909788166600.
4. Zhou, H.M., Zhang, J.G., Zhang, X. & Li, Q. Targeting cancer stem cells for reversing therapy resistance: mechanism, signaling, and prospective agents. *Signal Transduct. Target. Ther.* **6**, 62 (2021). https:://doi.org/10.1038/s41392-020-00430-1.
5. Mani, S.A., Guo, W., Liao, M.J., Eaton, E.N., Ayyanan, A., Zhou, A.Y., Brooks, M., Reinhard, F., Cheng, C.Z., Shipitsin, M. et al. The epithelial-mesenchymal transition generates cells with properties of stem cells. *Cell* **133**, 704-715 (2008). https://doi.org/10.1016/j.cell.2008.03.027.
6. Dart, A. EMT in chemoresistance. *Nat. Rev. Cancer* 2**3**, 349 (2023). https://doi.org/10.1038/s41568-023-00581-7.
7. Dong, J., Li, J., Li, Y., Ma, Z., Yu, Y. & Wang, C.Y. *Nat. Commun.* **12**, 3974 (2021). https://doi.org/10.1038/s41467-021-24137-1.
8. Hwyte, W.A., Orlando, D.A., Hnisz, D., Abraham, B.J., Lin, C.Y., Kagey, M.H., Rahl, P.B., Lee, T.I. & Young, R.A. *Cell* **153**, 309-319 (2013). https://doi.org/ 10.1016/j.cell.2013.03.035.
9. Hnis, D., Abraham, B., Lee, T.I., Lau, A., Saint-André, V., Sigova, A.A., Hoke, H.A. & Young, R.A. Super-enhancers in the control of cell identity and disease. *Cell* **155**, 934-947 (2013). https://doi.org/10.1016/j.cell.2013.09.053.

10. Sengupta, S. & George, R.E. Super-enhancer-driven transcriptional dependencies in cancer. *Trends Cancer* **3**, 269-281 (2017). https://doi.org/10.1016/j.trecan.2017.03.006.
11. Sabari, B.R., Dall'Agnese, A., Boija, A., Klein, I.A., Coffey, E.L., Shrinivas, K., Abraham, B.J., Hannett, N.M., Zamudio, A.V., Manteiga, J.C. et al. Coactivator condensation at super-enhancers links phase separation and gene control. *Science* **361**, eaar3958 (2018). https://doi.org/10.1126/science.
12. Tan, M., Pan, Q., Gong, H., Zhai, X., Wan, Z., Ge, M., Gu, J., Zhang, D., Chen, X. & Xu, D. Super-enhancer-associated SNHG15 cooperating with FOSL1 contributes to bladder cancer progression through the WNT pathway. *Pharmacol. Res.* **197**, 106940 (2023). https://doi.org/10.1016/j.phrs.2023.106940.
13. Luo, S., Luo, Y., Wang, Z., Yin, H., Wu, Q., Du, X. & Xie, X. Super-enhancer mediated upregulation of MYEOV suppresses ferroptosis in lung adenocarcinoma. *Cancer Lett.* **589**, 216811 (2024). https://doi.org/10.1016/j.canlet.2024.216811.
14. Hu, X., Wu, J., Feng, Y., Ma, H., Zhang, E., Zhang, C., Sun, Q., Wang, T., Ge, Y., Zong, D. et al. METTL3-stabilized super enhancers-lncRNA SUCLG2-AS1 mediates the formation of a long-range chromatin loop between enhancers and promoters of SOX2 in metastasis and radiosensitivity of nasopharyngeal carcinoma. *Clin. Transl. Med.* **13**, e1361 (2023). https://doi.org/10.1002/ctm2.1361.
15. Hazan, I., Monin, J., Bouwman, B.A.M., Crosetto, N. & Aqeilan, R.I. Activation of oncogenic super-enhancers is coupled with DNA repair by RAD51. *Cell Rep.* **15**, 560-572 (2019). https://doi.org/10.1016/j.celrep.2019.09.001.
16. Tasdemir, N., Banito, A., Roe, J.S., Alonso-Curbelo, D., Camiolo, M., Tschaharganeh, D.F., Huang, C.H., Aksoy, O., Bolden, J.E., Chen, C.C. et al. BRD4 connects enhancer remodeling to senescence immune surveillance. *Cancer Discov.* **6**, 612-629 (2016). https://doi.org/10.1158/2159-8290.CD-16-0217.

17. Li, G.H., Qu, Q., Qi, T.T., Teng, X.Q., Zhu, H.H., Wang, J.J., Lu, Q. & Qu, J. Super-enhancers: a new frontier for epigenetic modifiers in cancer chemoresistance. *J. Exp. Clin. Cancer Res.* **40**, 174 (2021). https://doi.org/10.1186/s13046-021-01974-y.
18. Zanconato, F., Cordenonsi, M. & Piccolo, S. YAP/TAZ at the roots of cancer. *Cancer Cell* **29**, 783-803 (2016). https://doi.org/10.1016/j.ccell.2016.05.005.
19. Zhao, B., Ye, X., Yu, J., Li, L., Li, W., Li, S., Yu, J., Lin, J.D., Wang, C.Y., Chinnaiyan, A.M. et al. TEAD mediates YAP-dependent gene induction and growth control. *Genes Dev.* **22**, 1962-1971 (2008). https://doi.org/10.1101/gad.1664408.
20. Zhang, H., Liu, C.Y., Zha, Z.Y., Zhao, B., Yao, J., Zhao, S., Xiong, Y., Lei, Q.Y. & Guan, K.L. TEAD transcription factors mediate the function of TAZ in cell growth and epithelial-mesenchymal transition. *J. Biol. Chem.* **284**, 13355-13362 (2009). https://doi.org/10.1074/jbc.M900843200.
21. Zheng, Y. & Pan, D. The Hippo signaling pathway in development and disease. *Dev. Cell* **50**, 264-282 (2019). https://doi.org/10.1016/j.devcel.2019.06.003.
22. Kim, M.H. & Kim, J. Role of YAP/TAZ transcriptional regulators in resistance to anti-cancer therapies. *Cell. Mol. Life Sci.* **74**, 1457-1474 (2017). https://doi.org/10.1007/s00018-016-2412-x.
23. Shao, D.D., Xue, W., Krall, E.B., Bhutkar, A., Piccioni, F., Wang, X., Schinzel, A.C., Sood, S., Rosenbluh, J., Kim, J.W. et al. KRAS and YAP1 converge to regulate EMT and tumor survival. *Cell* **158**, 171-184 (2014). https://doi.org/10.1016/j.cell.2014.06.004.
24. Lin, L., Sabnis, A.J., Chan, E., Olivas, V., Cade, L., Pazarentzos, E., Asthana, S., Neel, D., Yan, J.J., Lu, X. et al. The Hippo effector YAP promotes resistance to RAF- and MEK-targeted cancer therapies. *Nat. Genet.* **47**, 250-256 (2015). https://doi.org/10.1038/ng.3218.
25. Thrash, H.L. & Pendergast, A.M. Multi-functional regulation by YAP/TAZ signaling networks in tumor progression and metastasis. *Cancers* **15**, 4701 (2023). https://doi.org/10.3390/cancers15194701.

26. Zanconato, F., Forcato, M., Battilana, G., Azzolin, L., Quaranta, E., Bodega, B., Rosato, A., Bicciato, S., Cordenonsi, M. & Piccolo, S. Genome-wide association between YAP/TAZ/TEAD and AP-1 at enhancers drives oncogenic growth. *Nat. Cell Biol.* **17**, 1218-1227 (2015). https://doi.org/10.1038/ncb3216.
27. He, L., Pratt, H., Gao, M., Wei, F., Weng, Z. & Struhl, K. YAP and TAZ are transcriptional co-activators of AP-1 proteins and STAT3 during breast cellular transformation. *Elife* **10**, e67312 (2021). https://doi.org/10.7554/eLife.67312.
28. Galli, G.G., Carrara, M., Yuan, W.C., Valdes-Quezada, C., Gurung, B., Pepe-Mooney, B., Zhang, T., Geeven, G., Gray, N.S., de Laat, W. et al. YAP drives growth by controlling transcriptional pause release from dynamic enhancers. Mol. Cell **60**, 328-337 (2015). https://doi.org/10.1016/j.molcel.2015.09.001.
29. Kaan, H.Y.K., Chan, S.W., Tan, S.K.J., Guo, F., Lim, C.J., Hong, W. & Song, H. Crystal structure of TAZ-TEAD complex reveals a distinct interaction mode from that of YAP-TEAD complex. *Sci. Rep.* **7**, 2035 (2017). https://doi.org/10.1038/s41598-017-02219-9.
30. Khanal, P., Jia, Z. & Yang, X. Cysteine residues are essential for dimerization of Hippo pathway components YAP2L and TAZ. *Sci. Rep.* **8**, 3485 (2018). https://doi.org/10.1038/s41598-018-21828-6.
31. Sudol, M. YAP1 oncogene and its eight isoforms. *Oncogene* **32**, 3922 (2013). https://doi.org/10.1038/onc.2012.520.
32. Ben, C., Takahashi-Kanemitsu, A., Wu, X., Knight, C.K. & Hatakeyama, M. Alternative splicing reverses the cell-intrinsic and cell-extrinsic prooncogenic potentials of YAP1 via SHP2. *J. Biol. Chem.* **295**, 13965-13980 (2020). https://doi.org/10.1074/jbc.RA120.013820.
33. Bhamidipati, D., Haro-Silerio, J.I., Yap, T.A. & Ngoi, N. PARP inhibitors: enhancing efficacy through rational combinations. *Br. J. Cancer* **129**, 904-916 (2023). https://doi.org/10.1038/s41416-023-02326-7.

34. Kim, C., Wang, X.D. & Yu, Y. PARP1 inhibitors trigger innate immunity via PARP1 trapping-induced DNA damage response. *Elife* **9**, e60637 (2020). https://doi.org/10.7554/eLife.60637.
35. Gaffney, C.J., Oka, T., Mazack, V., Hilman, D., Gat, U., Muramatsu, T., Inazawa, J., Golden, A., Carey, D.J., Farooq, A. et al. Identification, basic characterization and evolutionary analysis of differentially spliced mRNA isoforms of human *YAP1* gene. *Gene* **509**, 215-222 (2012). https://doi.10.1016/j.gene.2012.08.025.
36. Ingham, R.J., Colwill, K., Howard, C., Dettwiler, S., Lim, C.S.H., Yu, J., Hersi, K., Raaijmakers, J., Gish, G., Mbamalu, G. et al. WW domains provide a platform for the assembly of multiprotein networks. *Mol. Cell. Biol.* **25**, 7092-7106 (2005). https://doi: 10.1128/MCB.25.16.7092-7106.2005
37. Kaneda, A., Seike, T., Danjo, T., Nakajima, T., Otsubo, N., Yamaguchi, D., Tsuji, Y., Hamaguchi, K., Yasunaga, M., Nishiya, Y. et al. The novel potent TEAD inhibitor, K-975, inhibits YAP1/TAZ-TEAD protein-protein interactions and exerts an anti-tumor effect on malignant pleural mesothelioma. *Am. J. Cancer Res.* **10**, 4399-4415 (2020).
38. Lu, Y., Wu, T., Gutman, O., Lu, H., Zhou, Q., Henis, Y.I. & Luo, X. Phase separation of TAZ compartmentalizes the transcription machinery to promote gene expression. *Nat. Cell Biol.* **22**, 453-464 (2020). https://doi.org/10.1038/s41556-020-0485-0.
39. Guo, Q., Quan, M., Dong, J., Bai, J., Wang, J., Han, R., Wang, W., Cai, Y. et al. The WW domains dictate isoform-specific regulation of YAP1 stability and pancreatic cancer cell malignancy. *Theranostics* **10**, 4422-4436 (2020). https://doi.org/10.7150/thno.42795.
40. Hatstat, A.K., Pupi, M.D. & McCafferty, D.G. Predicting PY motif-mediated protein-protein interactions in the Nedd4 family of ubiquitin ligases. *PLoS One* **16**, e0258315 (2021). https://doi.org/10.1371/journal.pone.0258315.

41. Mehta, S. & Zhang, J. Liquid-liquid phase separation drives cellular function and dysfunction in cancer. *Nat. Rev. Cancer* **22**, 239-252 (2022). https://doi.org/10.1038/s41568-022-00444-7.
42. Qian, H., Zhu, M., Tan, X., Zhang, Y., Liu, X. & Yang, L. Super-enhancers and the super-enhancer reader BRD4: tumorigenic factors and therapeutic targets. *Cell Death Discov.* **9**, 470 (2023). https://doi.org/10.1038/s41420-023-01775-6.
43. Conaway, R.C. & Conaway, J.W. Function and regulation of the mediator complex. *Curr. Opin. Genet. Dev.* **21**, 225-230 (2011). https://doi.org/10.1016/j.gde.2011.01.013.
44. Han, X., Yu, D., Gu, R., Jia, Y., Wang, Q., Jaganathan, A., Yang, X., Yu, M., Babault, N., Zhao, C. et al. Roles of the BRD4 short isoform in phase separation and active gene transcription. *Nat. Struct. Mol. Biol.* **27**, 333-341 (2020). https://doi.org/10.1038/s41594-020-0394-8.
45. Bacabac, M. & Xu, W. Oncogenic super-enhancers in cancer: mechanisms and therapeutic targets. *Cancer Metastasis Rev.* **42**, 471-480 (2023). https://doi.org/10.1007/s10555-023-10103-4.
46. Pérez-González, A.P., Bévant, K. & Blanpain, C. Cancer cell plasticity during tumor progression, metastasis and response to therapy. *Nat. Cancer* **8**, 1063-1082 (2023). https://doi.org/10.1038/s43018-023-00595-y.
47. Bocci, F., Gearhart-Serna, L., Boareto, M., Ribeiro, M., Ben-Jacob, E., Devi, G.R., Levine, H., Onuchic, J.N. & Jolly, M.K. Toward understanding cancer stem cell heterogeneity in the tumor microenvironment. *Proc. Natl. Acad. Sci. USA.* **116**, 148-157 (2019). https://doi.org/10.1073/pnas.1815345116.
48. Singh, A. & Settleman, J. EMT, cancer stem cells and drug resistance: an emerging axis of evil in the war on cancer. *Oncogene* **29**, 4741-4751 (2010). https://doi.org/10.1038/onc.2010.215.
49. Hu, J., Li, G., Zhang, P., Zhuang, X. & Hu, G. A CD44v^{+} subpopulation of breast cancer stem-like cells with enhanced lung metastasis capacity. *Cell Death Dis.* **8**, e2679 (2017). https://doi.org/10.1038/cddis.2017.72.

50. Nagano, O., Okazaki, S. & Saya, H. Redox regulation in stem-like cancer cells by CD44 variant isoforms. *Oncogene* **32**, 5191-5198 (2013). https://doi.org/10.1038/onc.2012.638.
51. Ceccaldi, R., Liu, J.C., Amunugama, R., Hajdu, I., Primack, B., Petalcorin, M.I., O'Connor, K.W., Konstantinopoulos, P.A., Elledge, S.J., Boulton, S.J. et al. Homologous-recombination-deficient tumours are dependent on Polθ-mediated repair. *Nature* **518**, 258-262 (2015). https://doi.org/10.1038/nature14184.
52. Baxter, J.S., Zatreanu, D., Pettitt, S.J. & Lord, C.J. Resistance to DNA repair inhibitors in cancer. *Mol. Oncol.* **16**, 3811-3827 (2022). https://doi.org/10.1002/1878-0261.13224.
53. Martinez-Cruzado, L., Tornin, J., Santos, L., Rodriguez, A., García-Castro, J., Morís, F. & Rodriguez, R. Aldh1 expression and activity increase during tumor evolution in sarcoma cancer stem cell populations. *Sci. Rep.* **6**, 27878 (2016). https://doi.org/10.1038/srep27878.
54. Filippakopoulos, P., Qi, J., Picaud, S., Shen, Y., Smith, W.B., Fedorov, O., Morse, E.M., Keates, T., Hickman, T.T., Felletar, I. et al. Selective inhibition of BET bromodomains. *Nature* **468**, 1067-1073 (2010). https://doi.org/10.1038/nature09504.
55. Zhang, C., Yang, Z., Dong, D.L., Jang, T.S., Knowles, J.C., Kim, H.W., Jin, G.Z. & Xuan, Y. 3D culture technologies of cancer stem cells: promising ex vivo tumor models. *J. Tissue Eng.* **11**, 1-17 (2020). https://doi.org/10.1177/2041731420933407.
56. Paolillo, M., Colombo, R., Serra, M., Belvisi, L., Papetti, A., Ciusani, E., Comincini, S. & Schinelli, S. Stem-like cancer cells in a dynamic 3D culture system: A model to study metastatic cell adhesion and anti-cancer drugs. *Cells* **8**, 1434 (2019). https://doi.org/10.3390/cells8111434.
57. Hanahan, D. & Weinberg, R.A. The hallmarks of cancer. *Cell* **100**, 57-70 (2000). https://doi.org/10.1016/s0092-8674(00)81683-9.
58. Cunningham, R. & Hansen, C.G. The Hippo pathway in cancer: YAP/TAZ and TEAD as therapeutic targets in cancer. *Clin. Sci. (Lond)* **136**, 197-222 (2022). https://doi.org/10.1042/CS20201474.

59. Pettitt, S.J., Frankum, J.R., Punta, M., Lise, S., Alexander, J., Chen, Y., Yap, T.A., Haider, S., Tutt, A.N.J. & Lord, C.J. Clinical *BRCA1/2* reversion analysis identifies hotspot mutations and predicted neoantigens associated with therapy resistance. *Cancer Discov.* **10**, 1475-1488 (2020). https://doi.org/10.1158/2159-8290.CD-19-1485.
60. Yan, Y., Zuo, X. & Wei, D. Concise review: Emerging role of CD44 in cancer stem cells: A promising biomarker and therapeutic target. *Stem Cells Transl. Med.* **4**, 1033-1043 (2015). https://doi.org/10.5966/sctm.2015-0048.
61. Wang, G., Lu, X., Dey, P., Deng, P., Wu, C.C., Jiang, S., Fang, Z., Zhao, K., Konaparthi, R., Hua, S. et al. Targeting YAP-dependent MDSC infiltration impairs tumor progression. *Cancer Discov.* **6**, 80-95 (2016). https://doi.org/10.1158/2159-8290.CD-15-0224.
62. Yang, W., Yang, S., Zhang, F., Cheng, F., Wang, X. & Rao, J. Influence of the Hippo-YAP signalling pathway on tumor associated macrophages (TAMs) and its implications on cancer immunosuppressive microenvironment. *Ann. Transl. Med.* **8**, 399 (2020). https://doi.org/10.21037/atm.2020.02.11.
63. Yu, M., Peng, Z., Qin, M., Liu, Y., Wang, J., Zhang, C., Lin, J., Dong, T., Wang, L., Li, S. et al. Interferon-γ induces tumor resistance to anti-PD-1 immunotherapy by promoting YAP phase separation. *Mol. Cell* **81**, 1216-1230 (2021). https://doi.org/10.1016/j.molcel.2021.01.010.
64. Yu, M., Peng, Z., Qin, M., Liu, Y., Wang, J., Zhang, C., Lin, J., Dong, T., Wang, L., Li, S. et al. Interferon-γ induces tumor resistance to anti-PD-1 immunotherapy by promoting YAP phase separation. *Mol. Cell* **81**, 1216-1230 (2021). https://doi.org/10.1016/j.molcel.2021.01.010.
65. Ooki, T., Murata-Kamiya, N., Takahashi-Kanemitsu, A., Wu, W. & Hatakeyama, M. High-Molecular-Weight hyaluronan is a Hippo pathway ligand directing cell density-dependent growth inhibition via PAR1b. *Dev. Cell* **49**, 590-604 (2019). https://doi.org/10.1016/j.devcel.2019.04.018.

66. Cerami, E., Gao, J., Dogrusoz, U., Gross, B.E., Sumer, S.O., Aksoy, B.A., Jacobsen, A., Byrne, C.J., Heuer, M.L., Larsson, E. et al. The cBio cancer genomics portal: an open platform for exploring multidimensional cancer genomics data. *Cancer Discov.* **2**, 401-404 (2012). https://doi.org/10.1158/2159-8290.
67. Gao, J., Aksoy, B.A., Dogrusoz, U., Dresdner, G., Gross, B., Sumer, S.O., Sun, Y., Jacobsen, A., Sinha, R., Larsson, E. et al. Integrative analysis of complex cancer genomics and clinical profiles using the cBioPortal. *Sci. Signal.* **6**, pl1 (2013). https://doi.org/10.1126/scisignal.2004088.
68. de Bruijn, I., Kundra, R., Mastrogiacomo, B., Tran, T.N., Sikina, L., Mazor, T., Li, X., Ochoa, A., Zhao, G., Lai, B. et al. Analysis and visualization of longitudinal genomic and clinical data from the AACR project GENIE Biopharma Collaborative in cBioPortal. *Cancer Res*. **83**, 3861-3867 (2023). https://doi.org/10.1158/0008-5472.CAN-23-0816.
69. Ryan, M., Wong, W.C., Brown, R., Akbani, R., Su, X., Broom, B., Melott, J. & Weinstein, J. TCGASpliceSeq a compendium of alternative mRNA splicing in cancer. *Nucleic Acids Res*. **44**, D1018-1122 (2016). https://doi.org/10.1093/nar/gkv1288.
70. Zhou, Y., Zhou, B., Pache, L., Chang, M., Khodabakhshi, A.H., Tanaseichuk, O., Benner, C. & Chanda, S.K. Metascape provides a biologist-oriented resource for the analysis of systems-level datasets. *Nat. Commun*. **10**, 1523 (2019). https://doi.org/10.1038/s41467-019-09234-6.

Acknowledgements

This work was supported by a JSPS Grant-in-Aid for Scientific Research from the Japan Society for the Promotion of Science Grant numbers 21H04804 (M.H.) 24H00618 (M.H), and JP21K15526 (T.O.), P-PROMOTE from AMED Grant Number JP23ama221219h0001 (M.H.), and Microbial Chemistry Research and Development Fund Grant Number 23A02 (T.O.).

Author contributions

T.O., T.H. (for Prediction of Molecular Complex Structure) and Y. Y. (for qPCR analysis) performed the experiments. T.O. and T.H. analyzed data. T.O. designed the study. T.O. and M.H. wrote the paper. T.H. reviewed the paper. M.H. supervised this work.

Competing interests

The authors declare no competing interests.

Additional information

Supplementary information

Supplemental Information includes 7 figures and 2 tables, can be found with this article online.

Correspondence

Further information and requests should be addressed to the lead contact, Masanori Hatakeyama (mhata@m.u-tokyo.ac.jp).

Figure Legends

Fig. 1 | Cancer cell resistance to genotoxic agents is associated with the upregulation of a minor YAP1 isoform, YAP1-2α. a RNA-seq analysis of PARPi-resistant MDA-MB-436 and UWB1.289 cells (n=3 per cell line). **b** Heat maps showing the changes in the expression of Hippo signaling-related genes. n=3 for each group. **c** Inclusion/exclusion of exon 6 in *YAP1* mRNA. Two independent PARPi-resistant cells (R1 and R2) for each *BRCA*-deficient cell line were used. **d**, **e** Comprehensive alternative splicing analysis. (**d**) Genes with altered exons and exon-exon junctions in PARPi-resistant cells. (**e**) Changes in *YAP1* exons and exon-exon junctions (left panel). Bar graphs indicate significantly altered exons (red lines) and exon-exon junctions (pink lines) (right panel). Exons 1 and 3 of *YAP1* were used as negative controls. **f** Three independent Cisplatin-resistant cell lines were established from UBW1.289 cells. MTS assay (top) and PCR analysis for exon 6 detection in *YAP1* mRNAs (bottom). **g** *BRCA*-deficient cells transduced with the indicated YAP1 isoforms using lentiviruses. Sensitivity of cells to Olaparib or Cisplatin (right). (**f**, **g**) Error bars indicate the mean ± SD. n=3.

Fig. 2 | Elevated YAP1-2α induces LLPS. a YAP1-immunofluorescence staining of PARPi-resistant UWB1.289 cells treated with or without Hex. The bottom panels are magnified images of the cells, as indicated by the yellow arrows in the top panels. **b** Immunoblotting of endogenous YAP1-1, YAP1-2, and mVenus-fused YAP1 isoforms. **c** The fluorescence signal

of mVenus (green). **d** Percentage of cells with nuclear YAP1 puncta is shown in (**c**). ***p < 0.001; n.s., not significant (Student's T test). n=3. Error bars indicate SEM. **e** Reconstitution of *YAP1*-knockout cells with a single YAP1 splicing isoform, YAP1-2α or YAP1-2γ (right panel). YAP1-2α-specific puncta formation was determined by immunofluorescence staining (left panel). **f**, **g** Live cell imaging of *YAP1*-KO UWB1.289 cells transfected with mVenus-fused YAP1-2α. (**f**) Yellow arrows indicate punctate fusion. (**g**) Fluorescence signals at the indicated time points after Hex treatment. **h**, **i** FRAP analysis of the mVenus-fused YAP1-2α. (**h**) Time-lapse images of two independent *YAP1*-KO UWB1.289 cells transfected with mVenus-fused YAP1-2α are shown in Exp.1 and Exp.2. Yellow arrows indicate photobleached puncta. Images of the entire nucleus are shown in Figure S2E. Unbleached puncta were used as negative controls. Scale bars indicate 1 μm. (**i**) Fluorescence intensities of puncta (photobleached, n=12; unbleached, n=12) were analyzed from a series of time-lapse images. τ: interval of fluorescence detection. Error bars indicate the mean ± SD. (**a**, **c**, **e**, **f**, **g**) Scale bars indicate 10 μm.

Fig. 3 | LLPS induced by the YAP1-2α/TAZ heterodimer activates a super-enhancer. a Nuclear puncta formation in *YAP1*-KO UWB1.289 cells expressing the mVenus-fused YAP1-2α mutants. **b** Interaction of YAP1-2α with TAZ, as visualized using PLA in UWB1.289 cells. Red dots: PL spots, green: mVenus fluorescence, yellow dots: colocalization of YAP1-

2α puncta and PL spots. **c** Formation of YAP1-2α puncta in the *TAZ*-KO MDA-MB-436 cells (left panel). Number of YAP1-2α puncta in the nucleus (right panel). **d**, **e** The Interaction of YAP1-2α mutants with TEAD was visualized using PLA. (**d**) Immunofluorescence images of mVenus-fused YAP1-2α (green) complexed with TEAD (red). The puncta indicated by white arrows are enlarged in the bottom row. (**e**) Co-localization of the YAP1-2α puncta and YAP1-2α/TEAD PL spots. Green circles: number of nuclear YAP1-2α puncta, red circles: number of nuclear PL spots, yellow circles: number of colocalized puncta and spots. n=20 nuclei. **f** Wild-type YAP1-2α(WT) or YAP1-2α(S94A)-transfected cells were treated with K-975. TEAD dependency of LLPS-mediated YAP1-2α puncta (left panel). Number of YAP1-2α puncta in the nucleus (right panel). (**a**, **c**, **f**) ***$p < 0.001$; **$p < 0.01$; n.s., not significant (**a**: ANOVA post Bonferroni, **c**, **f**: Student's T test). n=3. Error bars indicate the median ± SE. All scale bars represent 10 μm.

Fig. 4 | YAP1-2α/TAZ-induced super-enhancer formation requires TEAD and BRD4. a Puncta formation of YAP1-1α and YAP1-2α. Schematic diagrams of YAP1-1α and YAP1-2α (top panel). The fluorescence signal of mVenus (bottom left). Number of YAP1 puncta in the nucleus (bottom right). **b** Schematic diagram of BRD4. **c** Structural prediction of the interaction between YAP1-2α and BRD4 using AlphaFold2. The WW2 domain (grey), LPxY motif (blue), and PPxY motif

(magenta) are shown in the ribbon diagram (top). The vacuum electrostatic surface of the WW2 domain is represented in red (acidic) to blue (basic) (middle). The buried surface area of the LPxY and PPxY motifs in the complex (bottom). **d** Interaction between YAP1-2α and BRD4 in MDA-MB-436 cells. **e** Effect of BRD4 inhibition on YAP1-2α puncta formation in MDA-MB-436 cells. Cells transfected with shBRD4 were marked by GFP (green). mCherry-fused YAP1-2α (red). The cells indicated by white arrows were magnified, and the number of YAP1-2α puncta in the nucleus was calculated (top right). BRD4 was knocked down using two different shRNAs (#1 and #2) (bottom right). **f** Genetic rescue of the shBRD4-mediated reduction in YAP1-2α puncta formation by shBRD4-resistant BRD4. YAP1-2α (red), Flag-BRD4 (gray), nuclei (blue). The area indicated by the yellow dashed box is enlarged (bottom left). Yellow arrows indicate the colocalization of YAP1-2α puncta and BRD4. The number of YAP1-2α puncta in the nucleus is shown (right). (**a**, **e**, **f**) n=3, ***$p < 0.001$; **$p < 0.01$; *$p < 0.05$; n.s., not significant (**a**, **e**: Student's T test; **f**: ANOVA post Bonferroni). Error bars indicate the median ± SE. All scale bars represent 10 μm.

Fig. 5 | Rewiring of the transcriptional network by the YAP1-2α/TAZ/TEAD super-enhancer confers stem-like malignant properties. **a** Genes downregulated by BRD4 inhibition in MDA-MB-436 cells overexpressing YAP1-2α (left, n=3). BRD4 knockdown was confirmed by

immunoblotting (right). **b** LLPS dependence of the 932 genes upregulated by the YAP1-2α super-enhancer. Blue bars: fold increase (YAP1-2α/Control), black bars: fold decrease (shBRD4/shControl in YAP1-2α-overexpressing cells). **c** Genes upregulated in both PARPi-resistant and YAP1-2α-overexpressing MDA-MB-436 cells (left). Hallmark gene set analysis (right). **d** Pie charts showing CD44v9^{high} populations in parental UWB1.289 and MDA-MB-436 cells. **e** Qualitative splice variant analysis of *CD44* (top) and *YAP1* (bottom) mRNAs by PCR. **f** *YAP1-2α* mRNA and CD44v9 protein expression were detected using *in situ* RNA hybridization (BaseScope) and immunofluorescence staining, respectively. Scale bars represent 10μm. **g** qPCR analysis of *POLQ* (upper) and *ALDH1A3* (lower) mRNA expressions. n=3, ***$p < 0.001$; **$p < 0.01$, (Student's T test). Error bars indicate the median ± SD.

Fig. 6 | YAP1-2α/TAZ/TEAD super-enhancer induces cancer stem-like properties with elevated MMEJ activity. a-f Cells transfected with siControl or siPOLQ were subjected to the MMEJ reporter assay (**a-c**) or MTS assay (**d-f**). **a-c** The Effect of POLQ knockdown on MMEJ activity. (**a**) YAP1-2α-overexpressing MDA-MB-436 cells. (**b**) PARPi-resistant MDA-MB-436 cells. (**c**) CD44v^{high} UWB1.289 cells. **d-f** Sensitivity of cells to Olaparib or Cisplatin. (**d**) YAP1-2α-overexpressing MDA-MB-436 cells. (**e**) PARPi-resistant MDA-MB-436 cells. (**f**) CD44v^{high} UWB1.289 cells. See supplementary Fig. 6d for consideration of the off-target effects

of the siRNAs. **g** Sensitivities of CD44v^{high} UWB1.289 spheroids treated with K-975 or JQ1 to Olaparib or Cisplatin determined by 3D cell viability assay. **h** Growth of CD44v^{high} UWB1.289 spheroids treated with JQ1 or K-975, as measured by 3D cell viability assay (right). Bright-field images (left). Scale bars represent 200 μm. **i-k** 3D culture of CD44v^{high} UWB1.289 cells treated with or without JQ1. (**i**) Bright-field images of the spheroids. Scale bars represent 200 μm. (**j**) Three-dimensional reconstructed images of the spheroids. (**k**) Single-slice images of the spheroids. (**j**, **k**) Scale bars represent 10 μm. (**a**, **b**, **c**, **g**, **h**) ***$p < 0.001$; **$p < 0.01$; *$p < 0.05$. n.s., not significant (Student's T test). (**a-h**) Error bars indicate the mean ± SD. n=3.

Fig. 7 | The YAP1-2α/TAZ/TEAD super-enhancer strengthens cancer cell robustness and potentiates malignant characteristics. a-e YAP1-2α-overexpressing, YAP1-2γ-overexpressing, or PARPi-resistant UWB1.289 cells were treated with K-975 or JQ1. (**a**) Bright-field images and ki-67 staining of 3D-cultured spheroids. The Feret diameter of the spheroids is shown in the graph (bottom right). Red bars represent mean values. (**b**) Anchorage-independent 3D cell growth. (**c**) Invasion assay. (**d**) Migration assay. (**e**) Ferroptosis (left) and lipid hydroperoxide (right) assays. (**b-e**) n=3. Error bars indicate mean ± SD. **f-i** Sequential tissue sections derived from patients with high-grade serous ovarian cancer. (**f**) HE staining. (**g**) CD44v9 (magenta) and POLQ (green) staining. *YAP1-2α*

mRNA (red) was visualized using BaseScope. The dashed box area was enlarged (red box: tumor region in which *YAP1-2α*^{low} cells were enriched. Yellow box: the region in which both *YAP1-2α*^{high} and YAP1-2α^{low} tumor cells coexist in a mixture). (**h**) Correlation between the POLQ protein and *YAP1-2α* mRNA expression using scatter plots (r: Pearson's correlation coefficient). (**i**) Correlation between clinical stage and expression levels of *YAP1-2α* mRNA (left) or POLQ protein (right). The Boxes include the 25th–75th percentiles, with bars indicating means and whiskers indicating the range of data. **j** Overall survival rates of patients in TCGA cohort using Kaplan-Meier curves. Ovarian cancer (OV). Triple-negative breast cancer (TNBC). **k** Nude mice were subcutaneously inoculated with MKN45 gastric cancer cells ectopically expressing YAP1-2α(WT) or YAP1-2α(LZM). The dot plots show the tumor volumes measured 20 d after inoculation (n=12 for each group). Red bars indicate the mean tumor volumes. (**a**-**e**, **i**, **j**, **k**) ***$p < 0.001$; **$p < 0.01$; *$p < 0.05$; n.s., not significant (**a**-**d**: ANOVA post-Bonferroni, **e**, **i**, **k**: Student's T test, **j**: log-rank test). All scale bars represent 100 μm.

Figure 1.

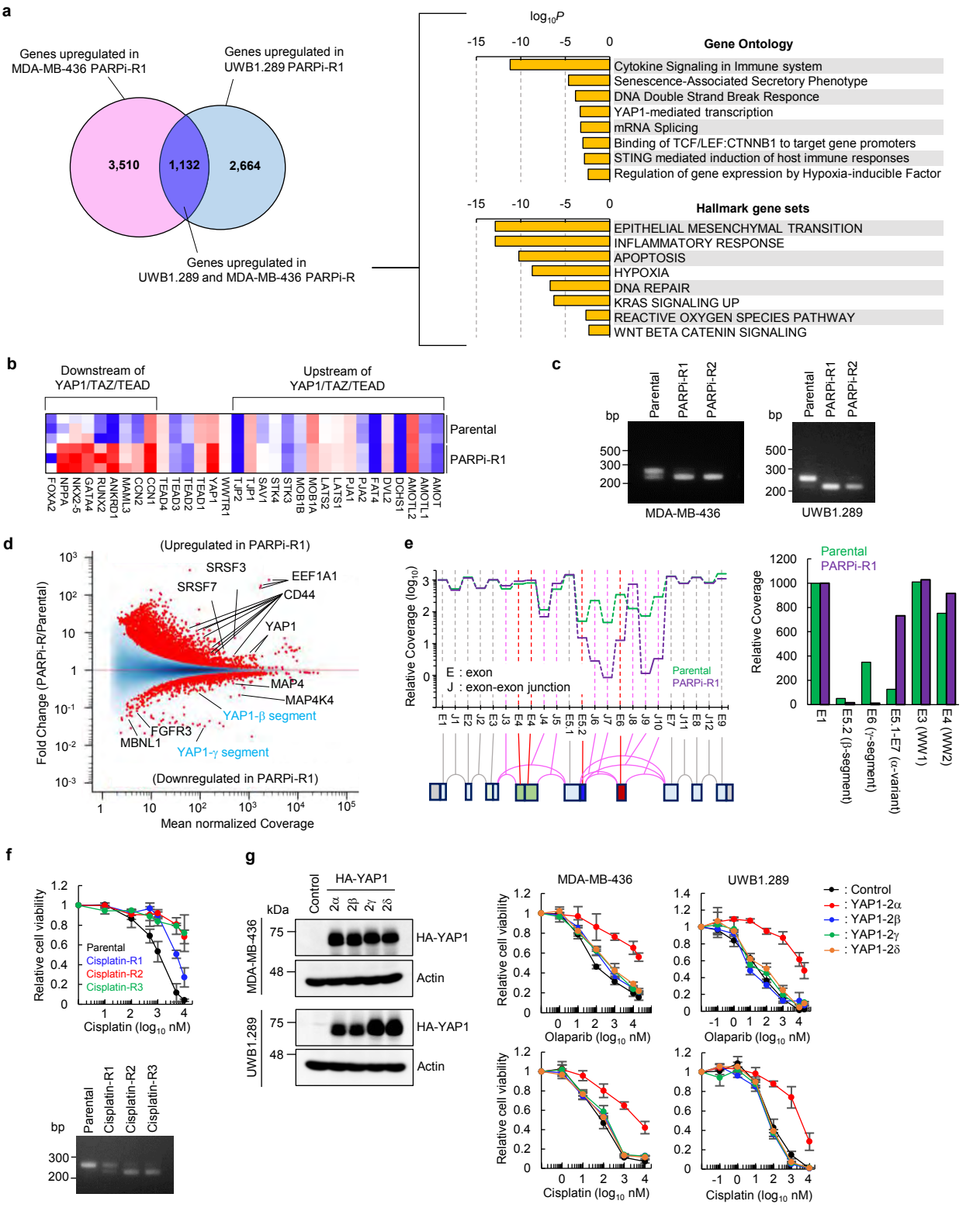
a
Genes upregulated in MDA-MB-436 PARPi-R1
Genes upregulated in UWB1.289 PARPi-R1
3,510
1,132
2,664
Genes upregulated in UWB1.289 and MDA-MB-436 PARPi-R
log10P
Gene Ontology
Cytokine Signaling in Immune system
Senescence-Associated Secretory Phenotype
DNA Double Strand Break Responce
YAP1-mediated transcription
mRNA Splicing
Binding of TCF/LEF:CTNNB1 to target gene promoters
STING mediated induction of host immune responses
Regulation of gene expression by Hypoxia-inducible Factor
Hallmark gene sets
EPITHELIAL MESENCHYMAL TRANSITION
INFLAMMATORY RESPONSE
APOPTOSIS
HYPOXIA
DNA REPAIR
KRAS SIGNALING UP
REACTIVE OXYGEN SPECIES PATHWAY
WNT BETA CATENIN SIGNALING
b
Downstream of YAP1/TAZ/TEAD
Upstream of YAP1/TAZ/TEAD
Parental
PARPi-R1
FOXA2 NPPA NKX2-5 GATA4 RUNX2 ANKRD1 MAML3 CCN2 CCN1 TEAD4 TEAD3 TEAD2 TEAD1 YAP1 WWTR1 TJP2 TJP1 SAV1 STK4 STK3 MOB1B MOB1A LATS2 LATS1 PJA1 PJA2 FAT4 DVL2 DCHS1 AMOTL2 AMOTL1 AMOT
c
Parental
PARPi-R1
PARPi-R2
bp
500
300
200
MDA-MB-436
UWB1.289
d
(Upregulated in PARPi-R1)
SRSF3
SRSF7
EEF1A1
CD44
YAP1
MAP4
MAP4K4
YAP1-β segment
FGFR3
MBNL1
YAP1-γ segment
(Downregulated in PARPi-R1)
Fold Change (PARPi-R/Parental)
Mean normalized Coverage
e
Relative Coverage (log10)
E : exon
J : exon-exon junction
Parental
PARPi-R1
Relative Coverage
E1
E5.2 (β-segment)
E6 (γ-segment)
E5.1-E7 (α-variant)
E3 (WW1)
E4 (WW2)
f
Relative cell viability
Parental
Cisplatin-R1
Cisplatin-R2
Cisplatin-R3
Cisplatin (log10 nM)
bp
300
200
g
Control
HA-YAP1
2α
2β
2γ
2δ
kDa
MDA-MB-436
UWB1.289
75
48
HA-YAP1
Actin
MDA-MB-436
UWB1.289
: Control
: YAP1-2α
: YAP1-2β
: YAP1-2γ
: YAP1-2δ
Olaparib (log10 nM)
Cisplatin (log10 nM)

Figure 2.

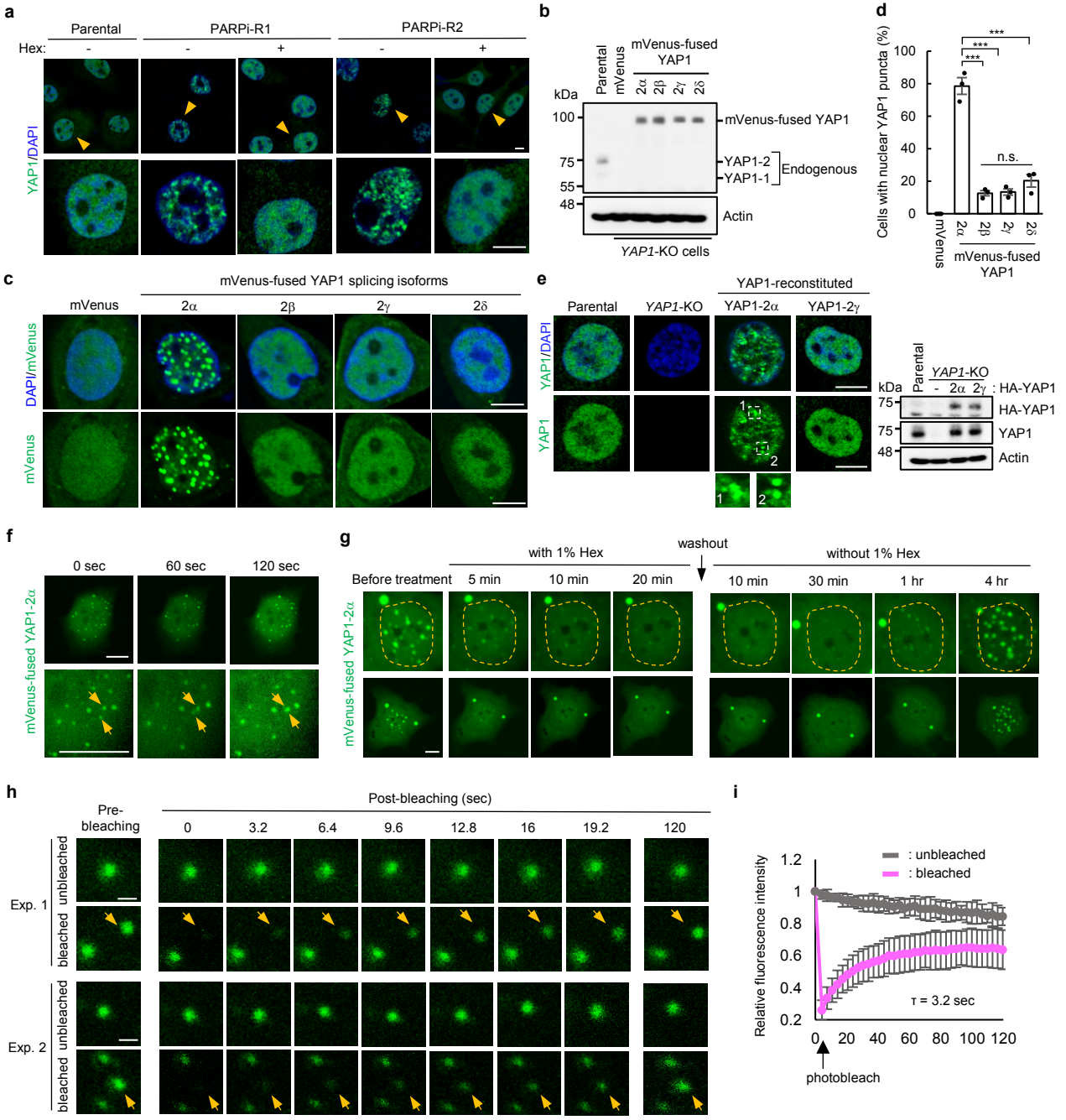
a
Parental
PARPi-R1
PARPi-R2
Hex:
YAP1/DAPI
b
Parental
mVenus
mVenus-fused YAP1
2α 2β 2γ 2δ
kDa
100
75
55
48
mVenus-fused YAP1
YAP1-2
YAP1-1
Endogenous
Actin
YAP1-KO cells
d
Cells with nuclear YAP1 puncta (%)
***
n.s.
mVenus
mVenus-fused YAP1
c
mVenus-fused YAP1 splicing isoforms
mVenus
2α 2β 2γ 2δ
DAPI/mVenus
mVenus
e
YAP1-reconstituted
Parental
YAP1-KO
YAP1-2α
YAP1-2γ
YAP1/DAPI
YAP1
HA-YAP1
f
0 sec
60 sec
120 sec
mVenus-fused YAP1-2α
g
with 1% Hex
washout
without 1% Hex
Before treatment
5 min
10 min
20 min
30 min
1 hr
4 hr
h
Pre-bleaching
Post-bleaching (sec)
0
3.2
6.4
9.6
12.8
16
19.2
120
Exp. 1
Exp. 2
unbleached
bleached
i
: unbleached
: bleached
Relative fluorescence intensity
τ = 3.2 sec
photobleach

Figure 3.

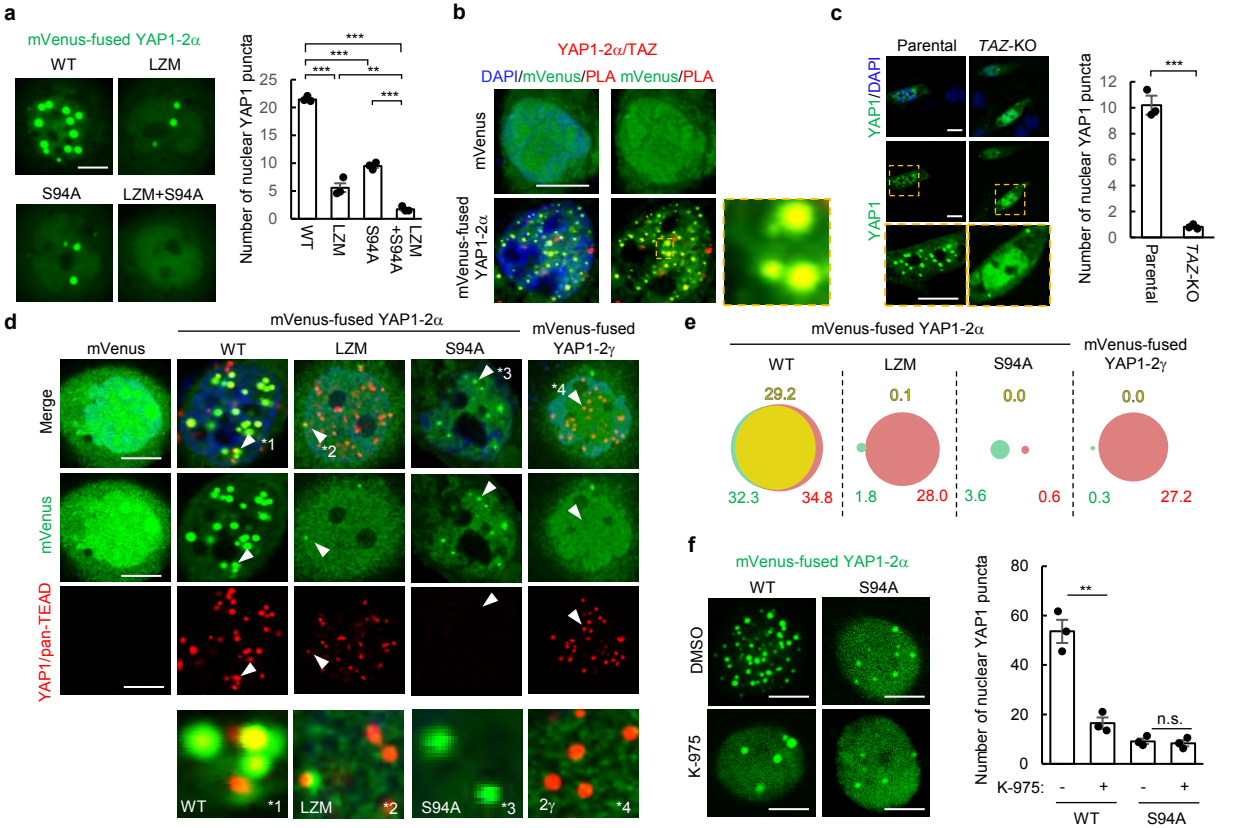
a
mVenus-fused YAP1-2α
WT
LZM
S94A
LZM+S94A
Number of nuclear YAP1 puncta
25
20
15
10
5
0
***
***
***
**
***
WT
LZM
S94A
LZM +S94A
b
YAP1-2α/TAZ
DAPI/mVenus/PLA mVenus/PLA
mVenus
mVenus-fused YAP1-2α
c
Parental
TAZ-KO
YAP1/DAPI
YAP1
Number of nuclear YAP1 puncta
12
10
8
6
4
2
0
***
Parental
TAZ-KO
d
mVenus-fused YAP1-2α
mVenus
WT
LZM
S94A
mVenus-fused YAP1-2γ
Merge
mVenus
YAP1/pan-TEAD
*1
*2
*3
*4
WT
LZM
S94A
2γ
e
mVenus-fused YAP1-2α
WT
LZM
S94A
mVenus-fused YAP1-2γ
29.2
32.3
34.8
0.1
1.8
28.0
0.0
3.6
0.6
0.0
0.3
27.2
f
mVenus-fused YAP1-2α
WT
S94A
DMSO
K-975
Number of nuclear YAP1 puncta
80
60
40
20
0
**
n.s.
K-975:
-
+
-
+
WT
S94A

Figure 4.

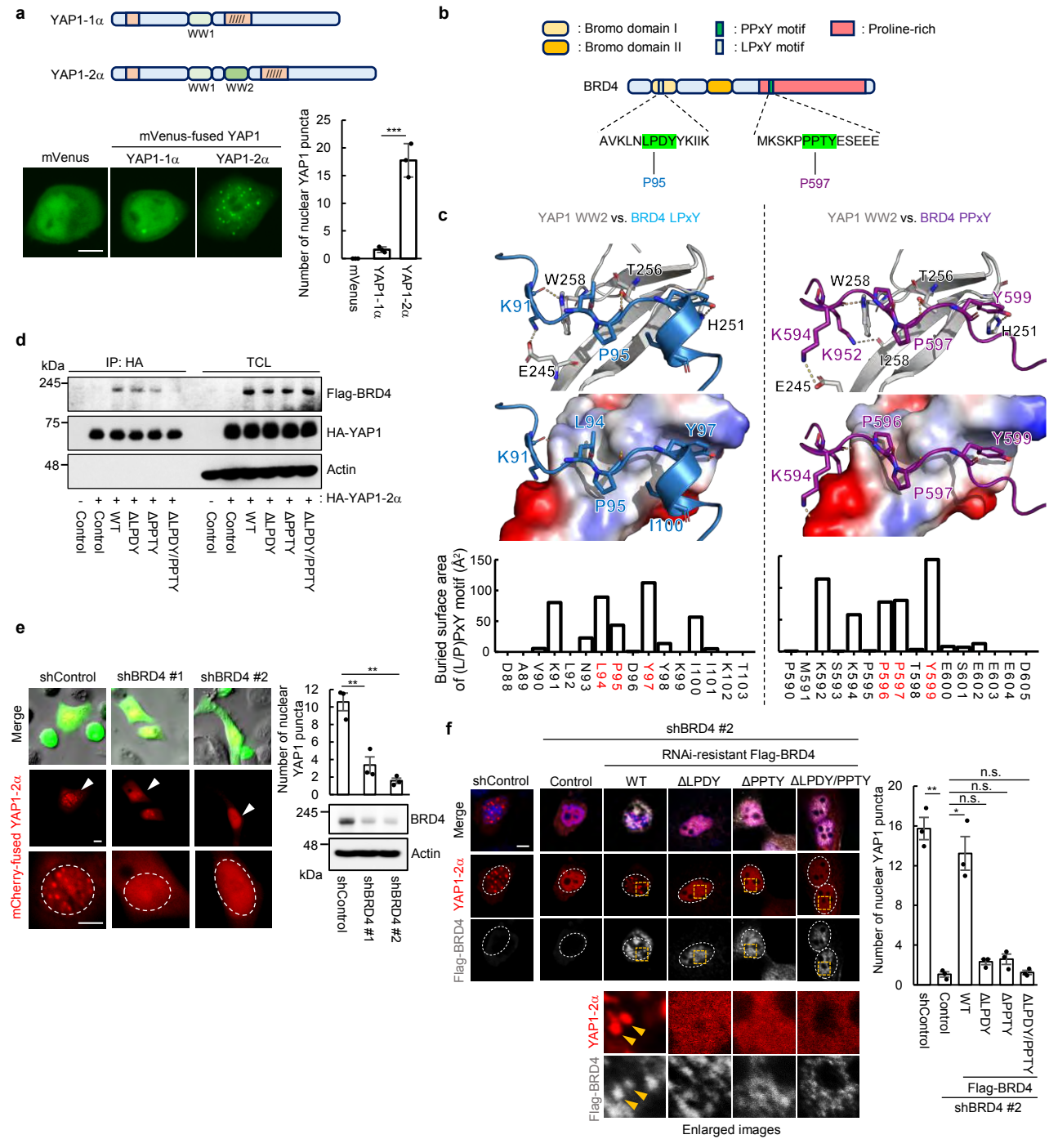
a
YAP1-1α
WW1
YAP1-2α
WW1 WW2
mVenus-fused YAP1
mVenus
YAP1-1α
YAP1-2α
Number of nuclear YAP1 puncta
mVenus
YAP1-1α
YAP1-2α
b
: Bromo domain I
: Bromo domain II
: PPxY motif
: LPxY motif
: Proline-rich
BRD4
AVKLNLPDYYKIIK
MKSKPPPTYESEEE
P95
P597
c
YAP1 WW2 vs. BRD4 LPxY
YAP1 WW2 vs. BRD4 PPxY
W258
T256
K91
H251
P95
E245
K594
K952
P597
I258
Y599
L94
Y97
I100
P596
Buried surface area of (L/P)PxY motif (Å²)
d
kDa
IP: HA
TCL
Flag-BRD4
HA-YAP1
Actin
: HA-YAP1-2α
Control
Control
WT
ΔLPDY
ΔPPTY
ΔLPDY/PPTY
e
shControl
shBRD4 #1
shBRD4 #2
Merge
mCherry-fused YAP1-2α
Number of nuclear YAP1 puncta
BRD4
Actin
kDa
f
shBRD4 #2
RNAi-resistant Flag-BRD4
shControl
Control
WT
ΔLPDY
ΔPPTY
ΔLPDY/PPTY
Merge
YAP1-2α
Flag-BRD4
Enlarged images
Number of nuclear YAP1 puncta
n.s.

Figure 5.

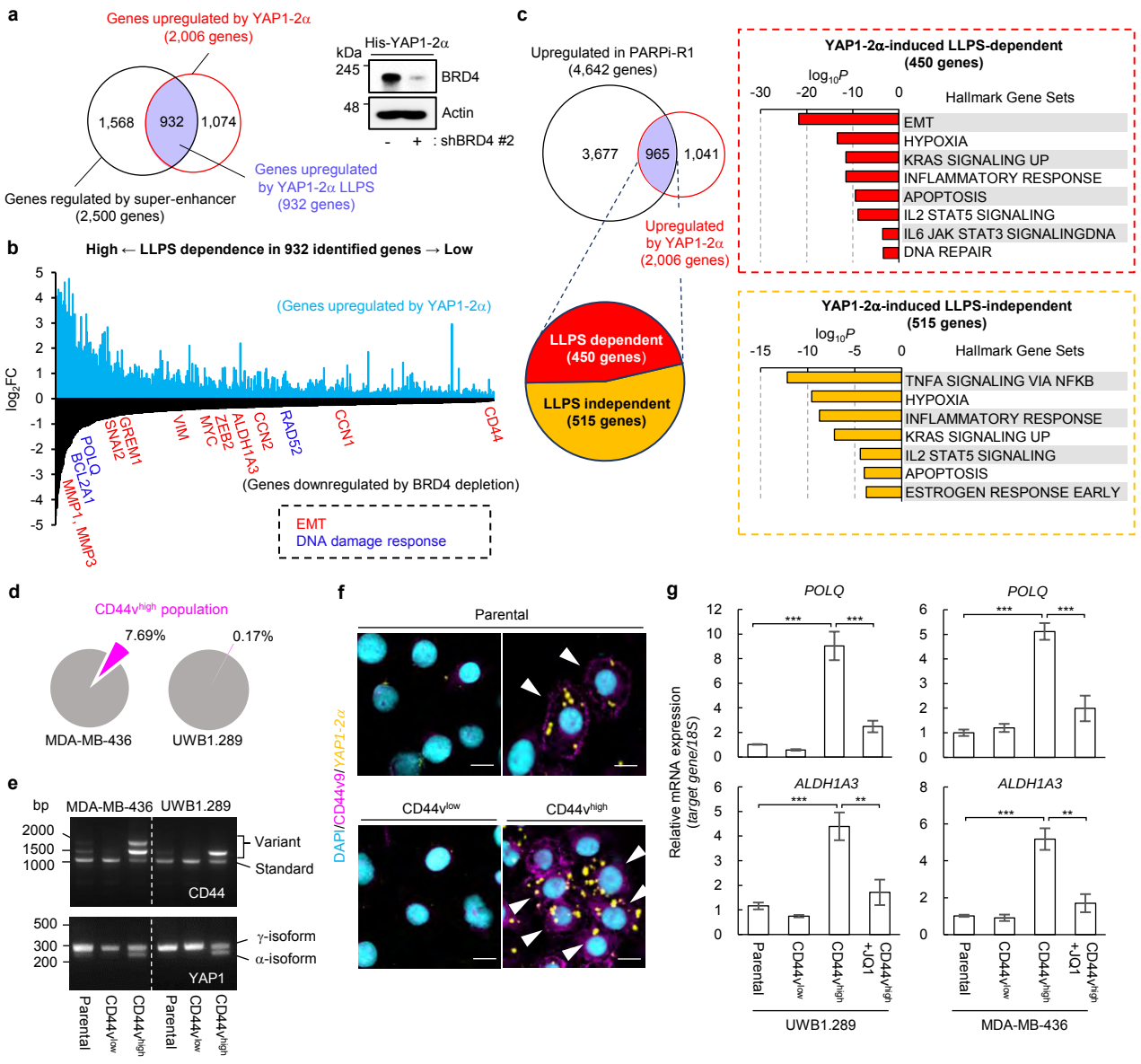
a
Genes upregulated by YAP1-2α (2,006 genes)
1,568
932
1,074
Genes regulated by super-enhancer (2,500 genes)
Genes upregulated by YAP1-2α LLPS (932 genes)
His-YAP1-2α
kDa
245
48
BRD4
Actin
- + : shBRD4 #2
b
High ← LLPS dependence in 932 identified genes → Low
log2FC
(Genes upregulated by YAP1-2α)
(Genes downregulated by BRD4 depletion)
POLQ
BCL2A1
MMP1, MMP3
SNAI2
GREM1
VIM
MYC
ZEB2
ALDH1A3
CCN2
RAD52
CCN1
CD44
EMT
DNA damage response
c
Upregulated in PARPi-R1 (4,642 genes)
3,677
965
1,041
Upregulated by YAP1-2α (2,006 genes)
LLPS dependent (450 genes)
LLPS independent (515 genes)
YAP1-2α-induced LLPS-dependent (450 genes)
log10P
Hallmark Gene Sets
EMT
HYPOXIA
KRAS SIGNALING UP
INFLAMMATORY RESPONSE
APOPTOSIS
IL2 STAT5 SIGNALING
IL6 JAK STAT3 SIGNALINGDNA
DNA REPAIR
YAP1-2α-induced LLPS-independent (515 genes)
TNFA SIGNALING VIA NFKB
HYPOXIA
INFLAMMATORY RESPONSE
KRAS SIGNALING UP
IL2 STAT5 SIGNALING
APOPTOSIS
ESTROGEN RESPONSE EARLY
d
CD44v high population
7.69%
0.17%
MDA-MB-436
UWB1.289
e
bp
MDA-MB-436
UWB1.289
Variant
Standard
CD44
γ-isoform
α-isoform
YAP1
Parental
CD44v low
CD44v high
f
Parental
CD44v low
CD44v high
DAPI/CD44v9/YAP1-2α
g
POLQ
ALDH1A3
Relative mRNA expression (target gene/18S)
+JQ1
UWB1.289
MDA-MB-436

Figure 6.

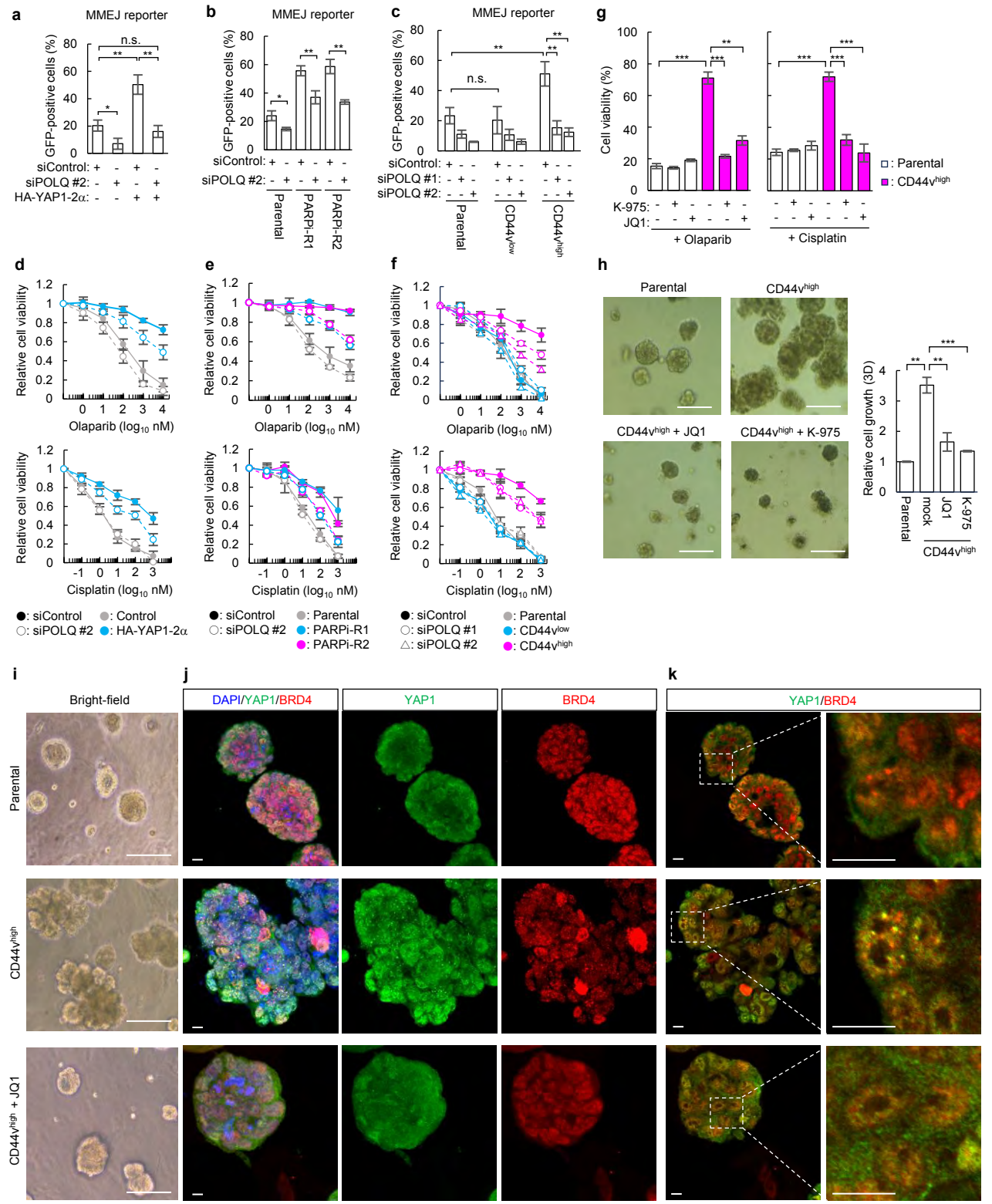
a
MMEJ reporter
GFP-positive cells (%)
n.s.
siControl:
siPOLQ #2:
HA-YAP1-2α:
b
MMEJ reporter
GFP-positive cells (%)
siControl:
siPOLQ #2:
Parental
PARPi-R1
PARPi-R2
c
MMEJ reporter
GFP-positive cells (%)
n.s.
siControl:
siPOLQ #1:
siPOLQ #2:
Parental
CD44v^low
CD44v^high
g
Cell viability (%)
K-975:
JQ1:
+ Olaparib
+ Cisplatin
: Parental
: CD44v^high
d
Relative cell viability
Olaparib (log10 nM)
Cisplatin (log10 nM)
: siControl
: siPOLQ #2
: Control
: HA-YAP1-2α
e
Relative cell viability
Olaparib (log10 nM)
Cisplatin (log10 nM)
: siControl
: siPOLQ #2
: Parental
: PARPi-R1
: PARPi-R2
f
Relative cell viability
Olaparib (log10 nM)
Cisplatin (log10 nM)
: siControl
: siPOLQ #1
: siPOLQ #2
: Parental
: CD44v^low
: CD44v^high
h
Parental
CD44v^high
CD44v^high + JQ1
CD44v^high + K-975
Relative cell growth (3D)
Parental
mock
JQ1
K-975
CD44v^high
i
Bright-field
Parental
CD44v^high
CD44v^high + JQ1
j
DAPI/YAP1/BRD4
YAP1
BRD4
k
YAP1/BRD4

Figure 7.

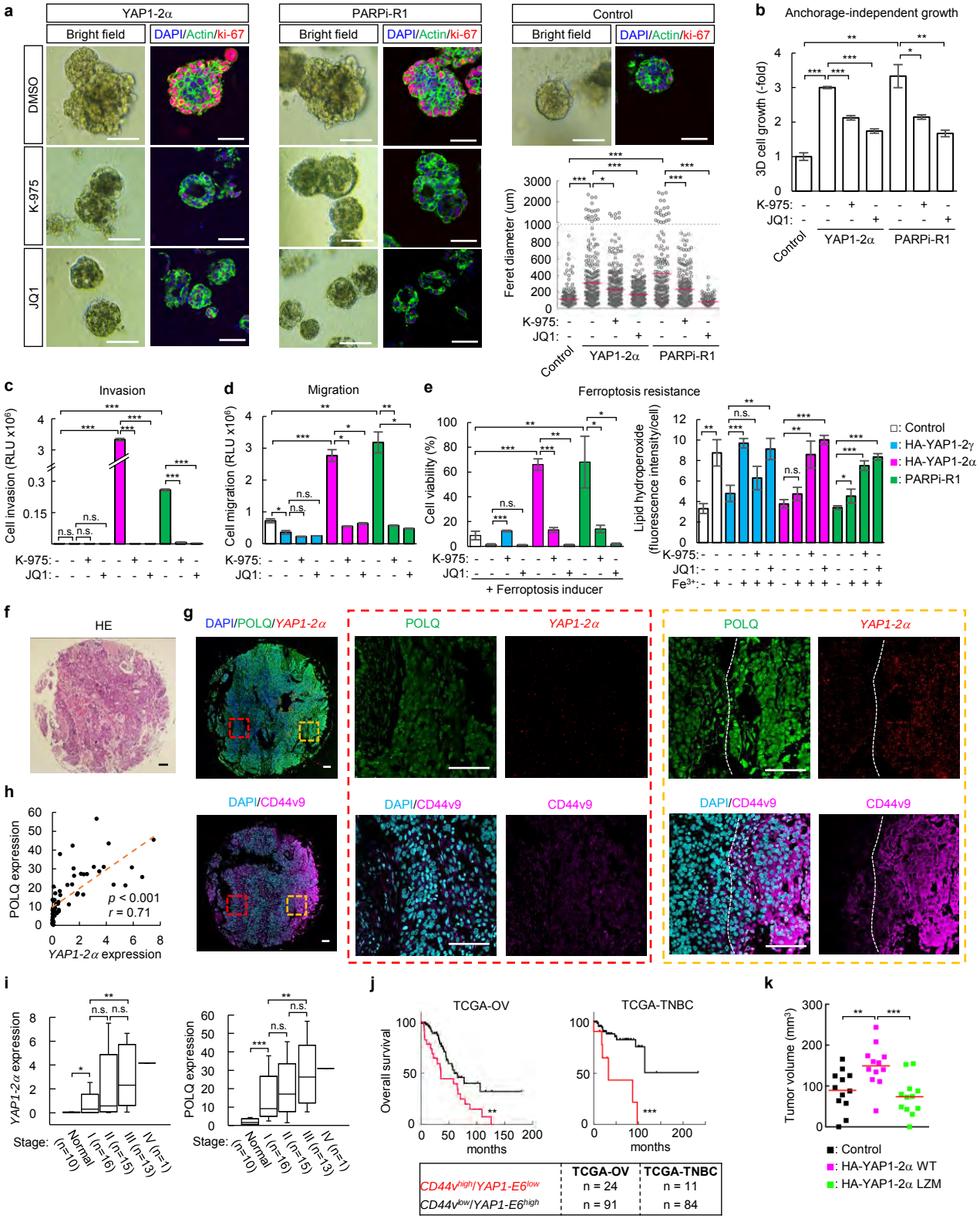

	TCGA-OV	TCGA-TNBC
CD44v^high/YAP1-E6^low	n = 24	n = 11
CD44v^low/YAP1-E6^high	n = 91	n = 84